

Evolution and differentiation of large icy moons

Piia Maria Tomberg

Lund Observatory
Lund University



2021-EXA184

Degree project of 60 higher education credits (for a degree of Master)
June 2021

Supervisor: Thomas Ronnet

Lund Observatory
Box 43
SE-221 00 Lund
Sweden

Abstract

Purpose: In preparation of several future missions with the objective to research the large icy moons of the Solar System, it is necessary to have a cohesive understanding of the conditions that might lead to the formation of liquid oceans in these moons. The purpose of this work is to create a numerical model for simulating the temperature evolution of the cores of large icy moons.

Method: Assuming 1-D spherical geometry, this work constructs a numerical model determining the energy and consequent temperature evolution in the rocky cores of large icy moons under the influence of radiogenic heating from ^{40}K , ^{235}U , ^{238}U and ^{232}Th . Both conductive and convective heat transfer methods were considered with different fractions of potassium present to account for the potential leaching of this element into the water layers above. The endothermic process of dehydrating clay minerals was also implemented in this model.

Results: Using the code the cores of Titan, Europa, Rhea and Mimas were simulated. It was determined that both core radius and remaining potassium fraction after leaching have significant effects on temperature evolution, with the highest possible temperatures reached in Titan with 100% of the potassium remaining at 3100 kelvins. However, using the often quoted fraction of 30% of the remaining potassium in the rocky cores, the temperatures in the cores of Titan and Europa are significantly lower, though continuing to increase at present day. When considering longer timescales, the core of Titan can undergo melting and subsequent metal-silicate differentiation even at the fraction of primordial potassium set to 30% of its original value.

Conclusions: Even with low amounts of potassium remaining in the rocky cores of Titan and Europa, the presence of an ocean on top of them remains very likely. Furthermore, radiogenic heating alone is sufficient to lead to full differentiation into a metallic core, a silicate outer core and an ice mantle, provided the potassium fraction in the core is sufficient.

Keywords: methods: numerical; conduction; convection; software: development; planets and satellites: interiors; planets and satellites: oceans.

Acknowledgements

I am very grateful to my supervisor, Thomas Ronnet, for the unfailing support and trust during this project, and the constant willingness for having involved discussions to improve my understanding of concepts involving physics, chemistry and even geology. I also extend a great thank you to Anders Johanssen for the advice on modelling the convection process and on the structural logic of the simulation code. I am very grateful to Florent Renaud, Paul McMillan, Alexander J. Mustill and Diane Feuillet for supporting me during the final weeks of writing the thesis. I am also immensely grateful to my family and my beets for supporting me through the entire thesis writing process.

Popular Science Summary

In the early 17th century when Galileo Galilei first decided to point a telescope at Jupiter, he noticed four faint objects placed around it on the same line. As he spent more and more nights viewing them he realised that instead of moving in the same direction as Jupiter these four objects in fact orbited the planet itself. This proved that it is possible for another body to be the centre of gravity for others, other than the Earth, challenging the widely spread tenets of that time.

These four objects are now known as the Galilean moons of Jupiter and three of them are classified as large icy moons because they consist in large part of ice, in addition to rocks. It is often thought that the rocky parts of these moons are gathered into a rocky core, leaving a thick ice mantle on top, but it is also possible for the rock and ice to be mixed up either throughout the entire moon or as an extra layer between a pure rocky core and pure ice mantle.

Since humans inevitably view the Universe from an Earth-centric point of view, we are fairly certain that liquid water is essential for the existence of life. This makes the large icy moons extremely interesting to planetary astronomy because if any of those moons are heated enough, it is possible for the ice to partially melt. This would form a liquid ocean somewhere in the thick ice mantle, making the large icy moons incredibly interesting to those in search of extraterrestrial life.

Large icy moons can be heated in several different ways, but the most important one by far is the heating from radioactive elements present in the rocky part of the moon. Since these generate heat they are often called radiogenic elements and since they are very long-lived, they have been heating the moons up to the present day since their formation 4 billion years ago! However, it is thought that during formation the ice was melted and well-mixed with the rocks and the water, which froze soon thereafter, absorbed a portion of one of the radiogenic elements: potassium. This process is called potassium leaching and because of this the ice mantle does not only get heated from the rocks below but also from within, making the formation of an ocean that much more likely!

This project involved writing a code to simulate these processes for several different large icy moons from the time of their formation to the present day and beyond. The most important parameter in these simulations is temperature since it defines the conditions in the ice, allowing for the possible formation of liquid oceans. In this work all large icy moons are concluded to be likely to host an ocean either now or in the future, with the largest ones like Titan even possibly having a metallic core having differentiated from the silicates similarly to how the rocks and ice differentiated.

Contents

1 Introduction	7
1.1 Composition	8
1.1.1 Ices	9
1.1.2 Oceans	9
1.1.3 Differentiation	10
1.2 Large icy moons of the solar system	10
1.3 Heating mechanisms	11
1.3.1 Radiogenic heating	11
1.3.2 Gravitational heating	12
1.3.3 Tidal heating	13
1.4 Methods of heat transport	13
1.4.1 Conduction	14
1.4.2 Convection	14
1.5 Effects of water	14
1.5.1 Potassium leaching	14
1.5.2 Dehydration	15
2 Method	16
2.1 Numerical model for core evolution	16
2.1.1 Implementation of potassium leaching	18
2.1.2 Implementation of dehydration in the rocky core	18
2.1.3 Viscosity and Rayleigh number of the rocky core	21
2.2 Radius of a hydrated rocky core	22
2.3 Analytical model for core evolution	23
2.4 Simulating convection in the rocky core	24
3 Results	25
3.1 Analytical model	25
3.2 Rhea and Mimas	26
3.3 Titan	27
3.4 Europa	29
3.5 Melting and convection of the core	31
3.5.1 Differences in the conductive and convective models	33
3.6 Onset of cooling in the rocky core	34
4 Discussion	36
4.1 Limitations of a purely conductive core model	36
4.2 Comparison of the convective and conductive model	37
4.3 Effects of potassium leaching	37
4.4 Assumed and actual Nusselt number	38
4.5 Effect of time step length and number of shells on results	38
4.6 Other heating mechanisms	40

5	Future developments	41
5.1	Surface temperature	41
5.2	Ice phases	42
5.3	Internal heating of the ice mantle	42
5.4	Core-mantle boundary	43
5.5	Silicate redistribution during dehydration	43
5.6	Differentiation	44
5.7	Initial conditions	44
6	Conclusions	45

List of Figures

1	Phase diagram of water, ice and higher pressure ice phases with the relevant points from Hobbs (1974) defining the phase change lines. . .	9
2	The modelled internal structure and composition of Europa, Ganymede, Callisto and Titan from Hussmann et al. (2015)	12
3	The heating power per volume of dry chondritic silicate of a selection of radiogenic elements relevant to the evolution of large icy moons, using data from Hevey and Sanders (2006) and Desch et al. (2009) . The heating power of ^{26}Al rapidly goes to 0. The heating power is shown from the end of the formation period at 10 Myr up to present day at 4000 Myr.	13
4	The integral of power, or the energy released by all the considered elements over time between 10–4000 Myr.	17
5	The differences between the numerical and analytical model for an object with the same parameters and heated only by ^{26}Al , at the centre ($0R$), halfway to the surface ($0.5R$) and near the surface at $0.9R$. (a) shows the recreated analytical solution from Hevey and Sanders (2006) in dashed lines overplotted with the numerical solution in solid lines. (b) shows the fractional difference between the models.	26
6	The temperature evolution in colour for Saturn’s moons Rhea and Mimas, exemplifying the difference in temperatures reached, depending on the core radii.	27
7	Titan’s thermal evolution in coloured dots with the hydration fraction shown in grayscale.	28
8	Titan’s thermal evolution in colour with 100% remaining potassium. .	29
9	Europa’s thermal evolution with 100% of the chondritic potassium remaining with the temperature in coloured dots and the hydration fraction in grayscale over a time period of 10 Gyr with the present day at 4 Gyr.	30
10	Europa’s thermal evolution in colour over a time period of 4 Gyr up to the present day with the plot above showing evolution with 100% of the chondritic potassium remaining in the core and the plot below with the estimated 30% potassium remaining. The temperature axis is joint for the two cases in order to emphasise the difference in temperature evolution.	31
11	The evolution of Nusselt’s number in Titan’s core in colour over a time period of 10 Gyr with the core radius on the y-axis and the time passed on the x-axis. White areas in the figure where the Nusselt number is not given represent a purely conductive regime where $Ra < 1000$ and the Nusselt number is not calculated.	32
12	The evolution of the volume fraction of melt in Titan’s core in colour over a time period of 10 Gyr with the core radius on the y-axis and the time passed on the x-axis. Melting occurs when in the red regions while blue regions at lower temperatures are considered solid.	33

13	Titan's core's evolution over 10 Gyr, showing the temperature difference between the conductive and convective models in colour.	34
14	Titan's core's evolution over 12 Gyr for different remaining potassium fractions, showing the temperature in colour.	35
15	The evolution of Titan's temperature and Rayleigh number for four different potassium leaching fractions, leaving, from left to right, 30, 50, 70 and 80% of the original potassium remaining. In the temperature plots (top row) the critical temperature is shown in a dashed line, above which the formula for viscosity (equation 15) must be changed to a liquid one. In the Rayleigh number plots (bottom row) the critical value of 1000, above which the conductive model becomes inaccurate, is shown as a dashed line.	36
16	The temperature difference when using Courant stability conditions of 1% - 5% and 5% - 10% as exemplified by the first 300 Myrs of Titan's evolution with 30% of chondritic potassium remaining.	39
17	The temperature difference when a simulation is run with 50 shells and 100 shells as exemplified by the first 500 Myrs of Titan's evolution with 30% of chondritic potassium remaining.	40

List of Tables

1	All the general parameters used in the numerical model for the thermal evolution of a rocky core.	19
2	Table of constants for calculating the viscosity of the rocky core.	22
3	Radii of the hydrated rocky cores of all moons considered in this work with references to the constants used to calculate them.	23
4	The values of constants used in equation 19	24

1 Introduction

The aim of this thesis is to construct a code for a numerical model of the thermal evolution of icy moons. This model includes the possible melting of both ice and silicates and takes into account several processes inherently connected to the presence of water with the silicates in the early stages of a large icy moon's lifetime.

Large icy moons are generally considered to be the Galilean moons of Jupiter, except the innermost Io, and Saturn's largest moon, Titan. These moons are of particular interest due to the possible presence of liquid water underneath their icy surfaces. While there is a general understanding of the interior of the large icy moons and their oceans (Schubert et al., 2004), the mechanisms leading to the formation and the durability of these oceans are however largely unknown. The oceans could be primordial in origin or they could have formed as a result of longer evolutionary processes. Research on the interior structures and processes of large icy moons has been historically limited by the scarcity of observational constraints to draw conclusions from. The first postulation of liquid oceans under the surfaces of these moons was made in the 1970s and has been explored to some extent up to present day (Kirk and Stevenson, 1987), (Spohn and Schubert, 2003).

The silicate cores of large icy moons share some similarities with smaller bodies such as Kuiper belt objects (Desch et al., 2009) and planetesimals (Hevey and Sanders, 2006), since these experience radiogenic heating as well. Due to the dual nature of large icy moons, both studies on internally heated and possibly convective silicate cores and works on melting ice mantles need to be unified for a complete understanding. More recent works, such as Castillo-Rogez and Lunine (2010), have modelled the silicate core and ice mantle, finding dehydration to be a relevant process, but not elaborating on possible convection or melting in the rocky core. Most studies involving large icy moons focus only on possible convection in the ice mantle such as Deschamps and Sotin (2001), who conclude that convection in a volatile-enriched ice mantle plays an important part in the cooling of icy satellites and may have contributed to a recent freezing of oceans. Spohn and Schubert (2003) also explore the complex phase diagram of volatile-enriched ice and show that a thick stagnant lid with poor thermal conductivity greatly increases the interior temperatures of the ice mantle and encourage ocean formation, however not considering the implications that the increased temperature may have on the rocky core.

Due to the temperature evolution that the rocky cores of large icy moons undergo, possible partial or complete melting should be considered, since it would lead to both the differentiation of a metallic core and more efficient heat transport to the ice mantle above. However, this is not considered for large icy moons, warranting the use of studies on the evolution of magma oceans (Solomatov, 2007) and on convective heat transport in silicates (Vilella et al., 2018). The detailed study on internally heated magma convection of Vilella et al. (2018) could be used for the evolution of the silicate cores as they are internally heated and may melt as well, in addition to

applicability to the ice mantle being internally heated by radiogenic elements present there. In this work the possible convective heat transport in the rocky cores of large icy moons is modelled similarly to [Desch et al. \(2009\)](#) where the thermal conductivity is increased from the intrinsic conductive value to simulate the more efficient heat transport method of convection. A convective rocky core is of particular interest in the formation and preservation of a liquid ocean on top of the rocky core since the more efficient method of heat transport would contribute to ocean formation more than conduction alone.

The evidence for liquid oceans in the large icy moons varies from plume material analysis from Enceladus ([Postberg et al., 2011](#)) to periodic changes in quadrupole gravity, indicating deformations characteristic to a subsurface ocean ([Iess et al., 2012](#)). In addition, Europa has been detected to have an induced magnetic field originating from close to its surface, which indicates the presence of a convective liquid ocean enriched by electrically conductive salts ([Khurana et al., 1998](#)). Also, Ganymede's aurorae could be affected by the presence of a deep electrically conductive ocean ([Saur et al., 2015](#)), which could be confirmed with the improved magnetic field observations that the JUICE mission will provide. In preparation for the multiple space exploration missions to characterise Jupiter's moons with the JUICE mission and for Europa in particular with NASA's mission sending the Europa Clipper, it is important to have a good understanding of the possible current structure of these icy moons.

In the remainder of this chapter a general overview of the composition, structure and common processes occurring in large icy moons are described. Specific emphasis is put on heating processes and mechanisms of heat transport, which directly affect the formation of liquid oceans. In chapter 2 the specific methods used to construct a numerical model is presented. In chapter 3 the results of several different simulations are given with comparison to a numerical model to check for correct implementation. In chapter 4 the uses and limitations of this model are discussed in addition to how the presence of liquid water in the late formation stages can affect the overall evolution of the moons. In chapter 5 several possible future developments that can be implemented in this work are discussed, including the addition of an ice mantle and the difficulties it presents. Finally, the conclusions of this thesis are presented in chapter 6.

1.1 Composition

Large icy moons initially consist of ices and silicates. The general assumption is that the silicates are of chondritic, or of early-solar-system composition ([Elkins-Tanton et al., 2011](#)). These silicates have been thoroughly studied from primordial meteorites, providing constraints on the amount of radioactive elements present at the formation of the Solar System. The ice of a large icy moon is often assumed to be pure water ice or enriched with possible volatiles, which would decrease the melting temperature of the ice, thus making the formation of oceans more conceivable ([Spohn and Schubert, 2003](#)). The ice mantle of the moon can then consist of both solid ices and liquids.

1.1.1 Ices

The phase diagram of water must be considered when the formation of a liquid ocean is plausible due to the change in pressure and temperature with depth. In this work the low pressure ice phase is called ice-I.

If the ice mantle of a moon is thick enough then there may be higher pressure (HP) ice phases present underneath an ice-I layer or an ocean. The different HP ice phases vary by density, structure, and most importantly, thermal conductivity. The phase diagram of pure water and its different ice phases, with the appropriate constants from [Hobbs \(1974\)](#) for phase changes are given in figure [1](#).

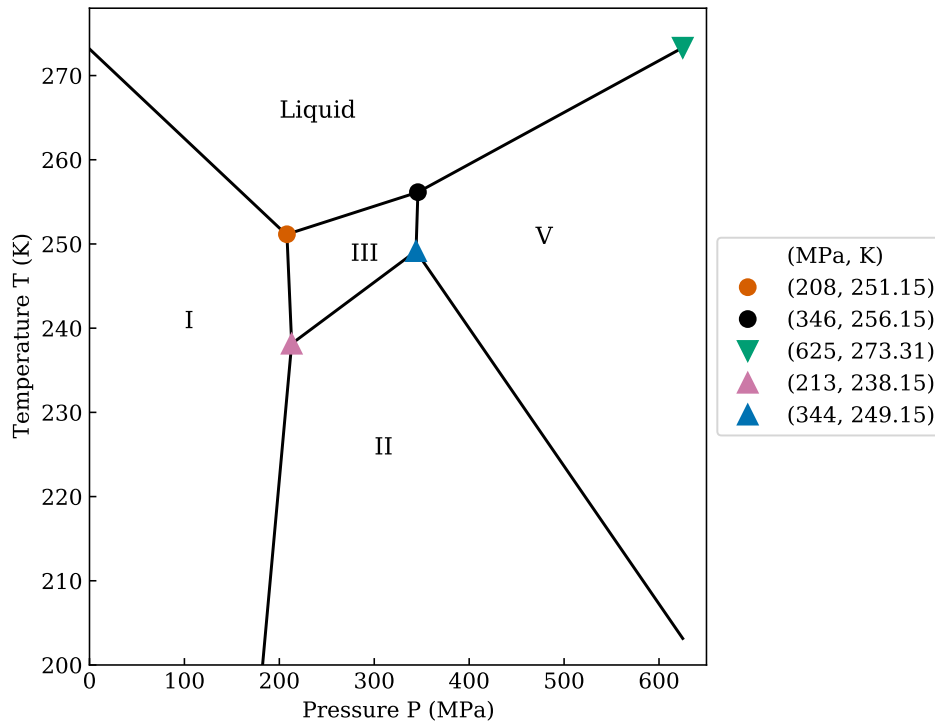


Figure 1: Phase diagram of water, ice and higher pressure ice phases with the relevant points from [Hobbs \(1974\)](#) defining the phase change lines.

1.1.2 Oceans

Water ice has an interesting phase diagram in the sense that the phase change from ice-I to liquid has a decreasing temperature with increasing pressure, therefore depth within a moon. This property makes the formation of an interior ocean more feasible as the temperature can be as low as 252 kelvins and still create an ocean if the needed pressure is achieved at a given depth.

The formation of an ocean can be made even more likely with the presence of volatiles in the ice mantle. Volatiles are chemical compounds, most importantly ammonia but

also methane and salts, which adjust the phase diagram to have an even lower melting temperature, the effect of which is determined by the concentration of volatiles present (Spohn and Schubert, 2003).

1.1.3 Differentiation

In a large icy moon it is possible for the ice and rock to have separated from each other, forming a rocky core and an ice mantle. If the temperatures in the resulting rocky core become high enough then it is also possible for the core to melt and form a metallic core, surrounded by a silicate outer core. In this case the moon is fully differentiated, like Jupiter's moons Europa and Ganymede are expected to be. If the temperatures in the core do not become high enough, the moon remains differentiated only by ice and silicate, such as Saturn's moon Titan likely is (Hussmann et al., 2015).

It is assumed that during formation the silicates and ices are mixed throughout the moon, making it undifferentiated. Only if high enough temperatures are reached, can these differentiate later on. If a large icy moon consists of a distinct core, an ice and silicate mixture mantle and an ice mantle, the moon is partially differentiated. If there is a distinct silicate core and an icy mantle, the moon is differentiated, and if there is also a distinct inner metallic core, the moon is fully differentiated.

1.2 Large icy moons of the solar system

The largest moons in the solar system are Saturn's largest moon Titan and the four Galilean moons of Jupiter: Io, Europa, Ganymede and Callisto. Of these five named moons all but Io contain significant amounts of water ice, making them interesting in the context of this work. Ganymede is expected to have a metallic core since it has been measured to have its own magnetic field. Europa is also likely to have a metallic core since the gravitational moments measured for it suggest full differentiation into a metallic core, silicate outer core and an ice mantle. The internal structures of some large icy moons are shown in figure 2. An induced magnetic field has also been detected around Europa, but since its source is much closer to its surface than a metallic core would create, it is likely caused by a liquid that is electrically conductive, so Europa is expected to currently have a liquid ocean (Hussmann et al., 2015)

The internal structure of the remaining four moons in consideration of this project is a challenge to determine. The internal structure is calculated from the gravitational moments, that are measured when passing close by a moon. The gravitational moments are measured by instruments close to the moon by the gravitational pull that different regions exert on the instrument. The most important moments describe the polar oblateness and the equatorial bulge, of which the former is best measured during a polar flyby and the latter with an equatorial flyby. The moments of inertia are compared to hydrostatic models of spherical bodies of varying density profiles in order to find the number of layers that have different densities. Both a fully differentiated (metallic inner core, silicate outer core, ice mantle) and a partially differentiated

(silicate core, silicate-ice mixture mantle and ice mantle) have three layers, but the former has significantly more mass concentrated in the centre than the latter. The general principle is that the more differentiated an object is, the more concentrated its gravitational effect is in the centre of the body, with the heaviest and most gravitating material being gathered there (Gao and Stevenson, 2013).

It is very difficult to manoeuvre a spacecraft the necessary number of times through the needed areas of the same moon, hence the data to form a full hydrostatic model of all the moons in question is incomplete (Hussmann et al., 2015). For this reason the exact internal structures are very uncertain for all the large moons. There is also the matter of hydrostatic models likely not being able to reliably and accurately describe the internal structure, since there are large possible errors attached to such models. This stems from the hydrostatic models all assuming the ideal case of hydrostatic equilibrium, which all moons slightly deviate from, causing large errors for the derived moments of inertia for slowly rotating bodies such as Titan and Callisto. (Gao and Stevenson, 2013). The data collected so far generally suggests a fully differentiated structure for all the large icy moons, allowing for possible partial differentiation for Titan and Callisto, though the internal structures of these two moons have the most uncertainties (Hussmann et al., 2015).

1.3 Heating mechanisms

When investigating the presence of an ocean inside an icy moon, the temperature profiles of their interiors are of special interest. There are several ways in which a smaller body can be heated and the importance of every mechanism is heavily dependent on the moons themselves and their orbital properties. The most commonly considered sources of heating for large icy moons are discussed as follows.

1.3.1 Radiogenic heating

Radiogenic heating, or ‘heating by radioactive decay,’ is generally the most important heating mechanism in large icy moons since it is present in any body of chondritic composition which includes radiogenic elements. Radiogenic heat is created when radioactive decay, which produces alpha, beta or gamma rays. These are absorbed by the atoms, increasing their thermal movement. Radioactive decay of an amount of radioactive material is described by exponential decay, which means that the energetic rays and therefore heat released is greatest at the beginning of the moon’s lifetime and continuously decreases. This does not however imply a decrease in temperature as the temperature is also determined by the moon’s ability to retain the energy released by the radioactive decay. Rather, the heating rate of the moon decreases as less and less radiogenic atoms remain.

In the entire lifetime of any large icy moons there are two sets of radiogenic elements to take into consideration. Those groups would be the short and long lived elements, with their half-lives defining the duration of their relevance. The heating

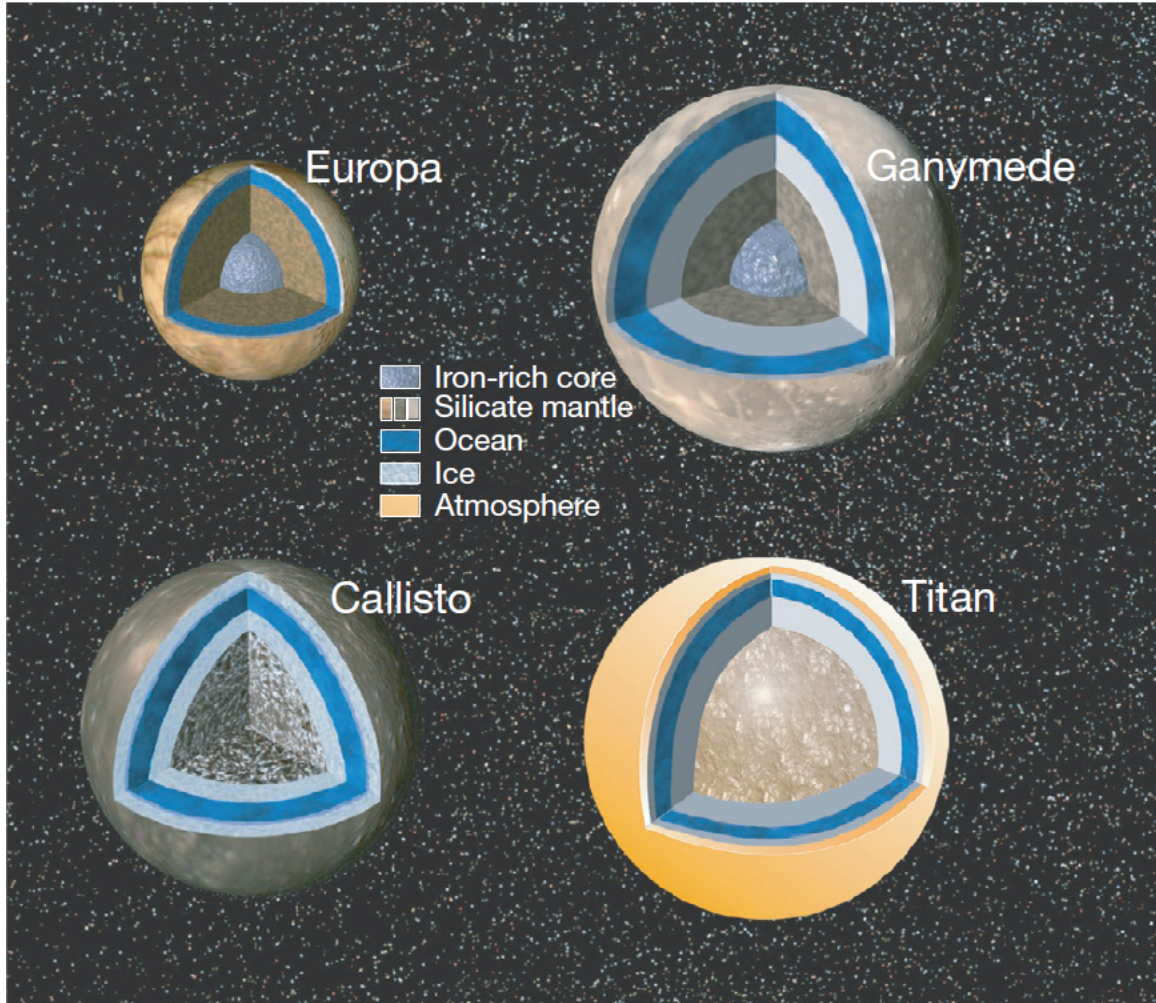


Figure 2: The modelled internal structure and composition of Europa, Ganymede, Callisto and Titan from [Hussmann et al. \(2015\)](#).

power of some radiogenic elements is shown in figure [3](#), from which it is apparent that ^{26}Al is a very short-lived radiogenic element compared to others such as uranium.

1.3.2 Gravitational heating

If a self-gravitating body is not fully differentiated but consists of a mixture of materials of different densities, the denser pieces gravitate towards the centre of the body, surrounding material's viscosity permitting. The heat is released as a consequence of a change in potential energy as a greater portion of the total mass of the object concentrates in the centre of the body, such as when undifferentiated rocky material separates from ices.

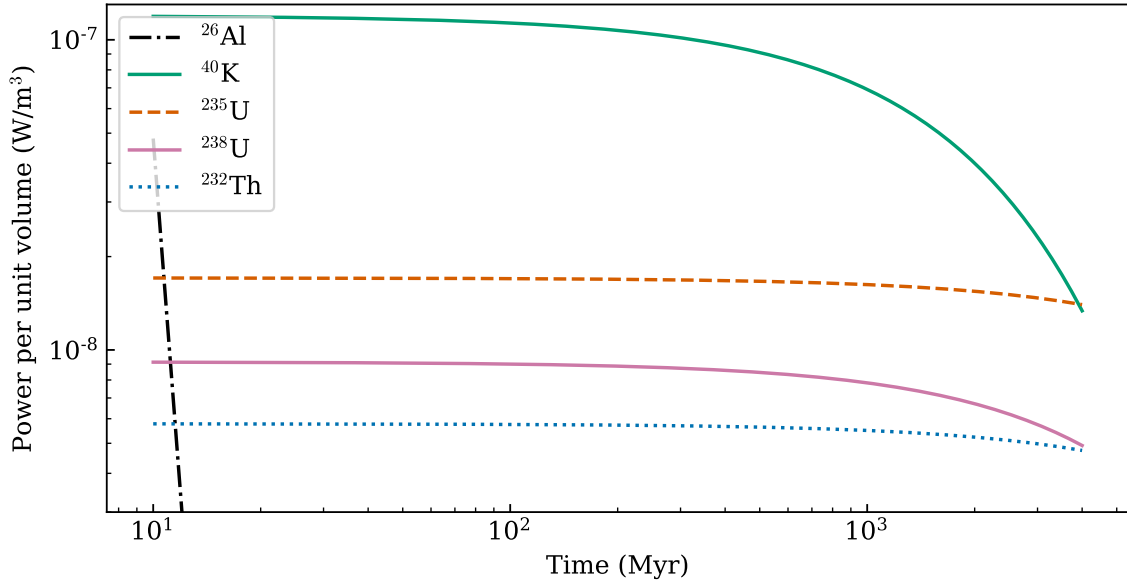


Figure 3: The heating power per volume of dry chondritic silicate of a selection of radiogenic elements relevant to the evolution of large icy moons, using data from Hevey and Sanders (2006) and Desch et al. (2009). The heating power of ^{26}Al rapidly goes to 0. The heating power is shown from the end of the formation period at 10 Myr up to present day at 4000 Myr.

1.3.3 Tidal heating

Tidal heating is a rarer form of heating that stems from the moon being subjected to a differential gravitational field slightly deforming it. This can only occur if the moon is both on an eccentric orbit and passes close enough to the host body for the difference in gravity to be large enough to have an impact. The body experiences tidal heating purely from the friction that is present during deformation, and is significant for only a few moons in the Solar System such as Io most importantly, but also Europa and Ganymede, all of which are Jupiter’s moons (Hussmann et al., 2015). It is thought that tidal heating plays an important role in the heating and ocean formation in Europa most specifically, but the importance of radiogenic heating in addition to it should also be considered.

1.4 Methods of heat transport

In any body where the temperature is not completely homogeneous there are heat transferring processes present, since the state of lowest energy for any body is to be in equilibrium with the surrounding temperature. It is apparent from the previous section on heating mechanisms that the moons are likely hotter than the space surrounding them. For this reason, a body that is heated in any way must be considered to have both conductive and possibly convective processes present.

1.4.1 Conduction

Conduction is the transfer of heat through material due to a difference in temperature, a process where efficacy is dependent only on the temperature difference and the material's thermal conductivity, k . Viscosity, η , which describes a material's capability to flow, is very low in conductive regions and since this form of heat transport is not the most efficient, if a conductive material is heated only from below, the temperature gradient with height is very steep.

1.4.2 Convection

Convection is a method of heat transport that occurs only if the viscosity of the material is low enough to allow for heated material to rise within the convecting layer, allowing for colder, upper regions to move downwards and become heated from below as well. Convection is often considered for a system that is heated from below, as then it becomes the most important method of heat transport, though roughly the same applies for a system that is heated both from below and internally.

Since the viscosity of a material is dependent on the temperature, with the lowest viscosity at high temperatures allowing for the most flow, the body must be heated to a high enough temperature for the material to become unstable to convection. Convection is inherently an unstable process, since within a convecting region there is a cyclic movement of material present. For this reason any convecting region is often considered to have a constant temperature, even though in reality the temperature gradient with increasing depth for a system considered to be in thermal equilibrium is an adiabatic increase in temperature with depth (Grasset and Sotin, 1996).

The importance of convection as a method of heat transport in a body can be quantified by the Rayleigh number. The Rayleigh number, defined in section 2.4 has a critical value of roughly $Ra = 10^3$ above which the viscosity is low enough and temperature high enough for the material to begin to convect.

1.5 Effects of water

The presence of liquid water introduces a perspective of chemical reactions related to water within a large icy moon. Since this project is primarily focused on physical processes, the chemical considerations are handled relying heavily on other works.

1.5.1 Potassium leaching

During the late formation stages of the large icy moons there is a significant enough amount of accretional heat present, in addition to heating from short-lived radiogenic elements such as ^{26}Al . This leads to much of the ice being in liquid form during this stage (Neveu et al., 2017). At that time it is therefore possible for radioactive isotopes present in the silicates to be leached into the liquid water (Hussmann et al., 2015). This is an important effect as it redistributes the heating power within the

entire large icy moons, reducing it in the silicate core and inserting it to the ice mantle.

The extent of potassium leaching is bounded by the thickness of the ice mantle and the percentage of its liquidity, also the surface area of silicates exposed to the liquid, and by the temperature of the liquid water. Since the most substantial radioactive element leached is potassium-40 (Kirk and Stevenson, 1987), most works focus only on that element (Castillo-Rogez and Lunine, 2010), (Neveu et al., 2017). Potassium leaching is most efficient at relatively low liquid temperatures (Neveu et al., 2017), indicating that high temperatures at the late formation stages lead to more potassium staying in the core and allowing it to evolve to higher temperatures. This is directly dependent on the formation timescale of the moon, with the fastest accretion rate reaching highest temperatures and allowing for less potassium leaching. The total amount of ice in a moon is determined by the formation time itself, since the circum-planetary disk must have cooled enough to allow for water to condense in the formation region of the moons (Barr and Canup, 2008).

1.5.2 Dehydration

During the formation of the moons the melting water likely results in the formation of hydrated silicates, such as those that are observed in some primitive meteorites. The most common component in these silicates is antigorite, the dehydration process of which is described in Castillo-Rogez and Lunine (2010). Dehydration occurs in two stages, with both being endothermic processes releasing water. The first stage is the most important one due to its specific heat being 367 kJ/kg compared to the second stage with a specific heat 37 times smaller at 10 kJ/kg. Both of these processes require a set temperature to be reached in order for dehydration to be triggered. These temperatures are, 743 K and 873 K respectively.

In essence, dehydration is a chemical process releasing, in addition to water, several silicate types, but since this work focuses on the formation of liquid oceans, it does not focus on the chemistry of the resulting silicates. The endothermic reaction of dehydration after being triggered by reaching the critical temperature will claim all the excess energy created in the silicates until the silicates become fully dehydrated, causing a noticeable lull in the thermal evolution of the cores of large icy moons.

2 Method

In this work it is assumed that during the early stages of a moon’s lifetime most of the ice is in a liquid state, which would lead to the differentiation of silicates from the water which later froze. For this reason the model for the rocky core is treated separately with an initially uniform temperature of 300 kelvins and the core’s surface temperature set to a constant 300 K throughout the simulation, following (Castillo-Rogez and Lunine, 2010). The early differentiation process would also have hydrated the silicates in the rocky core and potentially leached a significant amount of radioactive ^{40}K , redistributing the most influential heating element into the ice mantle as well as the core.

In this chapter the various models used to simulate icy moons are described in detail. Initially, the numerical model for the thermal evolution of the rocky core is described, including processes such as dehydration, potassium leaching and instability to convection. This is followed by a brief description of the analytical model which the numerical model was compared to.

2.1 Numerical model for core evolution

The numerical model of the rocky core assumes a spherical symmetry, dividing the core into N shells. The source of energy is considered to be only radiogenic heating from ^{40}K , ^{26}Al , ^{235}U , ^{238}U and ^{232}Th following

$$Q_i(t) = H_0 \cdot e^{-\lambda t} \cdot m_i, \quad (1)$$

where H_0 is the heat output from a single element per unit mass of silicates at the time of formation, λ is the decay constant, and m_i is the mass of shell i , defined as $m_i = \frac{4}{3}\pi(r_i^3 - r_{i-1}^3)$. The half-lives of the considered radiogenic elements are 1.265 Gyr for ^{40}K , 0.729 Myr ^{26}Al , 0.704 Gyr for ^{235}U , 4.47 Gyr for ^{238}U and 14.0 Gyr for ^{232}Th

In the silicate cores of icy moons ^{40}K is the most important source of energy and ^{26}Al is not considered due to its extremely short half-life compared to the other radiogenic elements. Large icy moons must have finished accretion during the late stages of the host planet’s formation in order to accrete ices, so no earlier than 4 Myr before the formation of the solar system (Barr and Canup, 2008). However, due to the short-lived nature of ^{26}Al , it is not a relevant source of heat after a moon’s formation, as can be seen in figure 3. The energy released by ^{26}Al is greatest at timescales shorter than 10 Myr since the beginning of the Solar system, thus it can be expected to be relevant only during the late formation stages, as the simulations run in this work have an initial time of 10 Myr. This is further shown in figure 4 where the energy created by ^{26}Al at times after 10 Myr is negligible compared to the other elements. This was calculated by integrating the power given in equation 1.

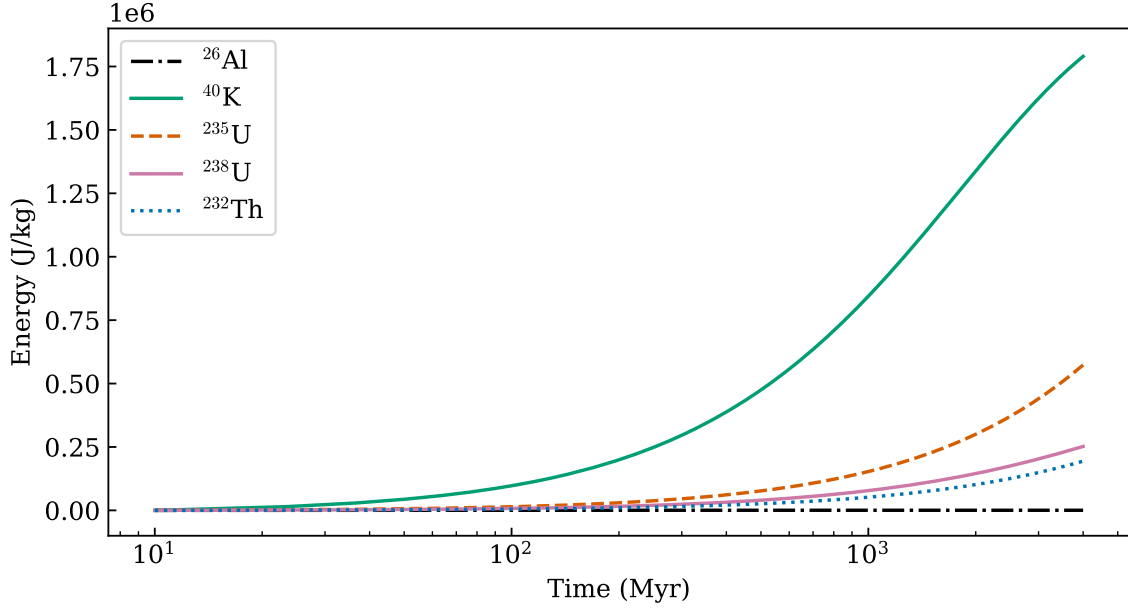


Figure 4: The integral of power, or the energy released by all the considered elements over time between 10–4000 Myr.

For heating from several elements, the energy is summed over the elements. The H_0 for each element is assumed to be the same in all icy moons, assuming chondritic abundances calculated by Lodders (2003) in the early solar system as described in appendix A of Desch et al. (2009). Due to potassium leaching possibly redistributing some of the ^{40}K to the ice mantle, the initial amount of it is varied and explored later on.

The numerical model is created based on Desch et al. (2009) where a change in internal energy over time is defined as

$$\frac{dE_i}{dt} = \frac{E_i(t + \Delta t) - E_i(t)}{\Delta t} = Q_i(t) + 4\pi r_{i-1}^2 F_{i-1} - r_i^2 F_i \quad (2)$$

where $Q_i(t)$ is defined in equation 1, the second term is the heat flux into shell i and the third term is the heat flux out of shell i where the flux is expressed as

$$F_i = -k \frac{T_{i+1} - T_i}{(r_{i+1} - r_{i-1})/2} \quad (3)$$

where k is a thermal conductivity that is assumed to be constant. Two boundary conditions must be addressed, the centre and the surface of the core. In the centre of the core $i = 0$, thus making the heat flux into the shell 0, leaving only the exiting heat flux for the innermost shell. The surface of the core was set to a constant temperature $T_N = 300$ K, thus setting the flux leaving the outermost layer to

$$F_{N-1} = k \frac{T_N - T_{N-1}}{(R - r_{N-2})/2}, \quad (4)$$

where T_N is the same as the core-mantle boundary temperature T_{CMB} given in table [1](#). Using equation [2](#) and multiplying it by the length of a single time step we find the energy generated in each shell, E , at one time step. The energy is conserved over time by comparing to the shell mass and heat capacity of the previous time step as

$$E_i = \frac{dE_i}{dt} \cdot \Delta t + E_{i,\text{old}} \cdot \left(\frac{m_i}{m_{i,\text{old}}} \cdot \frac{c_{p_i}}{c_{p_{i,\text{old}}}} \right). \quad (5)$$

The energy generated can be used to find the temperature of each shell by using the specific heat capacity, c_p as an equation of state as

$$T_i = \frac{E}{c_p \cdot m_i}, \quad (6)$$

where m_i is the mass of shell i , as described before.

The length of a variable time step was set using the Courant condition for stability, defined in [Desch et al. \(2009\)](#) as

$$\Delta t < \min \left[\frac{(\Delta r)^2}{2\kappa} \right], \quad (7)$$

Where κ is the thermal diffusivity and is given in table [1](#). Thermal diffusivity can be calculated from thermal conductivity as $\kappa = k/(c_p \cdot \rho)$. Due to the changes in all the components of thermal diffusivity over the shell radii, the minimum necessary time step was chosen and recalculated at the end of every time step, making it variable over time. Since this condition gives the maximum time step to ensure numerical stability, a value of 1% the Courant condition was used as the time step for the simulation. The length of a time step was thus separately calculated to ensure the stability of the simulation.

2.1.1 Implementation of potassium leaching

The percentage of potassium leached from the core in the early stages of a moon's lifetime is a subject of debate, with assumptions varying from 30% ([Kirk and Stevenson, 1987](#)) to even 100% ([Castillo-Rogez and Lunine, 2010](#)).

The effects of this process were implemented by assuming a lower-than-chondritic abundance of ^{40}K , assumed at 30% of the chondritic composition, though variances of the leached amount were also considered. As can be seen in section [4.3](#) this has a profound impact on the thermal evolution of a rocky core.

2.1.2 Implementation of dehydration in the rocky core

As described in section [1.5.2](#), the rocky contents of a moon are hydrated during formation. If the core reaches high enough temperatures, a chemical reaction called dehydration takes place, claiming energy and inhibiting further heating, separating the water from the silicates. According to [Castillo-Rogez and Lunine \(2010\)](#) at the

Table 1: All the general parameters used in the numerical model for the thermal evolution of a rocky core.

Term	Symbol	Unit	Value
Surface temperature	T_{CMB}	K	300
Thermal conductivity	k	$\text{W m}^{-1}\text{K}^{-1}$	4.2
Thermal diffusivity	κ	$\text{m}^2 \text{s}^{-1}$	$2.97 \cdot 10^{-7}$
^{26}Al decay constant	λ_{Al}	s^{-1}	$3.012 \cdot 10^{-14}$
^{40}K decay constant	λ_{K}	s^{-1}	$1.736 \cdot 10^{-17}$
^{235}U decay constant	$\lambda_{^{235}\text{U}}$	s^{-1}	$1.569 \cdot 10^{-18}$
^{238}U decay constant	$\lambda_{^{238}\text{U}}$	s^{-1}	$4.914 \cdot 10^{-18}$
^{232}Th decay constant	λ_{Th}	s^{-1}	$1.569 \cdot 10^{-18}$
^{26}Al initial power per unit volume	$H_{0,\text{Al}}$	W kg^{-1}	$1.9 \cdot 10^{-7}$
^{40}K initial power per unit volume	$H_{0,\text{K}}$	W kg^{-1}	$35.2 \cdot 10^{-12}$
^{235}U initial power per unit volume	$H_{0,^{235}\text{U}}$	W kg^{-1}	$5.02 \cdot 10^{-12}$
^{238}U initial power per unit volume	$H_{0,^{238}\text{U}}$	W kg^{-1}	$2.68 \cdot 10^{-12}$
^{232}Th initial power per unit volume	$H_{0,\text{Th}}$	W kg^{-1}	$1.70 \cdot 10^{-12}$
Hydrated silicate density	ρ_{hy}	kg m^{-3}	2520
Anhydrous silicate density	ρ_{dry}	kg m^{-3}	3400
Specific heat capacity of hydrated silicates	$c_{p,\text{hy}}$	$\text{J kg}^{-1} \text{K}^{-1}$	2000
Specific heat capacity of anhydrous silicates	$c_{p,\text{dry}}$	$\text{J kg}^{-1} \text{K}^{-1}$	900
Isothermal bulk modulus	K_0	Pa	$126.3 \cdot 10^9$
Derivative of K_0	K'_0		4.2
Thermal expansion coefficient	α_ν	K^{-1}	$5 \cdot 10^{-5}$
Latent heat of dehydration	L	J kg^{-1}	$3.67 \cdot 10^5$

pressure of Titan’s core, dehydration starts once the temperature of 743 K is reached.

As dehydration is an endothermic process, it will claim all the energy generated in a shell, keeping the temperature at 743 K, until the entire shell has dehydrated. The reaction has a latent heat of $L = 367 \text{ kJ/kg}$, which gives the mass of dehydrated silicates obtained as a result of dehydration in a single time step as

$$M_{\text{dried}} = 0.87 \cdot M_{\text{converted}} = 0.87 \cdot \frac{Q}{L}, \quad (8)$$

where Q is the heat generated within a dehydrating time step. Here it is assumed that the water released by this process is immediately transported to the outside of the core, diminishing the total radius of the core.

Since hydrated and dehydrated silicates have different densities and specific heat capacities, these must be accounted for during the simulation. While dehydration is ongoing, the density and specific heat capacities in a shell are averaged, using mass hydration fraction X as a weight for the calculation. The change in density and loss of water also leads to a mass change in a shell during dehydration. The numerical model is set up so that the pure dry silicate mass in each shell is preserved over time.

If we assume that a fraction X of the mass of a shell is dehydrated and hydrated silicates contain 13% water, then the mass of a shell is defined as

$$m_{\text{shell}} = m_0(1 - 0.13X)$$

where m_0 is the mass of the shell during the previous timestep. The masses of hydrated and dry silicates in the shell are, respectively, $m_{\text{hy}} = (1 - X)m_{\text{shell}}$ and $m_{\text{dry}} = Xm_{\text{shell}}$. In order to find the average hydration-dependent density, the volume of the shell must be found as well, as

$$\begin{aligned} V_{\text{shell}} &= V_{\text{hy}} + V_{\text{dry}} = \frac{m_{\text{hy}}}{\rho_{\text{hy}}} + \frac{m_{\text{dry}}}{\rho_{\text{dry}}} = \frac{(1 - X)m_{\text{shell}}}{\rho_{\text{hy}}} + \frac{X \cdot m_{\text{shell}}}{\rho_{\text{dry}}} = \\ &= m_{\text{shell}} \left(\frac{1 - X}{\rho_{\text{hy}}} + \frac{X}{\rho_{\text{dry}}} \right), \end{aligned}$$

where ρ_{hy} and ρ_{dry} are given in table [1](#). Thus, the *average* density of the shell is

$$\bar{\rho} = \left(\frac{1 - X}{\rho_{\text{hy}}} + \frac{X}{\rho_{\text{dry}}} \right)^{-1}. \quad (9)$$

Since the densities of both the hydrated and anhydrous silicates are dependent on pressure and temperature, these were calculated for each silicate shell following [Castillo-Rogez and Lunine \(2010\)](#), where the density of a shell ρ_i is dependent on the density, pressure and temperature of the shell above, ρ_{i+1} , P_{i+1} and T_{i+1} respectively, as

$$\bar{\rho}(P, T) = \rho_{i+1}(T_{i+1}, P_{i+1}) \cdot \left[\frac{K'_0(P_i - P_{i+1})}{K_0} + 1 \right]^{1/K'_0} [1 - \alpha_{av}(T_i - T_{i+1})], \quad (10)$$

where $\rho_{i+1}(T_{i+1}, P_{i+1})$ is the averaged shell density given in equation [9](#), dependent on temperature and pressure. K_0 , K'_0 and α_{av} are the isothermal bulk modulus, its derivative with respect to pressure and the thermal expansivity, with their values reported in table [1](#). Since the density of each shell is dependent on the shell above, the densities for all shells were calculated iteratively from the outside in during each time step when dehydration occurs.

The pressure in a shell is dependent on the radius of the shell as

$$P(R_i) = \frac{2\pi}{3} \cdot G \cdot \bar{\rho}(P, T)^2 (R_{\text{core}}^2 - R_i^2) + \frac{2\pi}{3} \cdot G \cdot \rho_{\text{ice}}^2 (R_{\text{total}}^2 - R_{\text{core}}^2) \quad (11)$$

where $\bar{\rho}(P, T)$ is the same density that is given in equation [10](#), R and r are the radii of the edges of a shell, and $\rho_{\text{ice}} = 1000 \text{ kg m}^{-3}$ is the assumed average ice density. The second half of the equation represents the additional pressure from the ice layer, where both the total and core radii are recalculated in every time step where dehydration occurs. Since dehydration changes the density and thus the volume of each shell ($V_{\text{shell}} = m_{\text{shell}}/\bar{\rho}(P, T)$), the radii of the shells must also be recalculated iteratively from the inside out as

$$\begin{aligned} R_0 &= \left(\frac{3V_0}{4\pi} \right)^{1/3} \\ R_i &= \left(\frac{3V_i}{4\pi} + R_{i-1}^3 \right)^{1/3}, \end{aligned} \quad (12)$$

where R_0 is the radius of the centremost sphere and R_i the radii of the other shells numbered from the inside out and calculated using the radius of the shell below, R_{i-1} . Recalculating this for each shell will give the new core radius, allowing for the total radius to be recalculated taking into account the released water/ice as

$$R_{\text{total}} = \left[3 \frac{(M_{\text{ice}} + \sum_{i=0} (m_{\text{shell},i} \cdot 0.13 \cdot (1 - X_i)))}{4\pi \cdot \rho_{\text{ice}}} + R_{\text{core}}^3 \right]^{1/3}, \quad (13)$$

where M_{ice} is the ice mantle mass of the previous time step, $\rho_{\text{ice}} = 1000 \text{ kg/m}^3$ and $m_{\text{shell},i}$ and X_i the masses and hydration fractions of all shells.

In order to keep track of these changes in density and radii, the total mass of the moon was calculated in each time step to ensure the conservation of mass.

2.1.3 Viscosity and Rayleigh number of the rocky core

Since the rocky core of a moon can be heated to high temperatures, it is possible that the silicates may experience a lowered viscosity and begin to melt. Thus, the density of these hotter and melted silicates becomes lower than that of the solid layers above, beginning to rise as the denser and colder silicates above start to sink. When a large enough fraction of silicates have melted this gives rise to convection, rendering the conductive model of heat transport in the core inaccurate.

The Rayleigh number is a dimensionless number which indicates the strength of convection in a substance. The Rayleigh number was used to track the onset of convection in every shell at each time step and was assumed to be significant once it surpasses the critical value of $Ra_{\text{crit}} = 10^3$.

The Rayleigh number was defined in [Solomatov \(2007\)](#) as

$$Ra = \frac{\alpha_{\nu} g (T_i - T_{i+1}) L^3}{\kappa \nu}, \quad (14)$$

where α_{ν} and κ are the thermal expansion coefficient and thermal diffusivity given in table [1](#), T_i is the temperature of the current shell, T_{i+1} is the temperature of the shell above, L is the thickness of the shell, $g = (GM)/R_i^2$, where R_i is the distance to the centre and M the enclosed mass. ν is the kinematic viscosity, defined with the standard viscosity, η , as $\nu = \eta/\rho$, where ρ is the local density, defined in equation [10](#).

The definition of viscosity, η , depends on whether the material is solid- or fluidlike, defined respectively as

$$\begin{aligned} \eta_{\text{sol}} &= \eta_s \exp(-\alpha_{\eta} \phi); & \phi &= \frac{T - T_{\text{sol}}}{T_{\text{liq}} - T_{\text{sol}}} \\ \eta_{\text{liq}} &= \frac{\eta_l}{\left(1 - \frac{(1-\phi)}{\phi_m}\right)^{2.5}} \end{aligned} \quad (15)$$

where ϕ is the volume fraction of melted material, so $1 - \phi$ in the second equation is the volume fraction of solid material. The constant $\phi_m = 0.64$ is the maximum crystal packing fraction which corresponds to the crystal state where all solid crystals are in contact with each other, beginning to behave more liquid-like. Thus the critical value of ϕ is $\phi_{\text{crit}} = 0.36$. This critical fraction marks the transition from a fluid-like to a solid-like behaviour in the mixture with the transition occurring at the critical temperature of 1637.5 kelvins. At temperatures lower than that the material behaves more like a solid and at higher temperatures more like a liquid. The behaviour of the silicates is only in question between the solidus temperature T_{sol} and liquidus temperature T_{liq} , since silicates with $T < T_{\text{sol}}$ are completely solid and silicates with $T > T_{\text{liq}}$ are completely liquid.

From equation [15](#) it is apparent that the viscosity is dependent on temperature, decreasing rapidly as temperature increases, thus facilitating the onset of convection, indicated by the increase of the Rayleigh number. Since these two equations for viscosity are dependent on temperature, the choice of which to use depends on a critical temperature where the two equations converge. This was found to be at $T_{\text{crit}} = 1637.5\text{K}$ using the bisection method, however there remains significant uncertainties on the precise viscosity of the silicates, which also depend on their exact composition. When calculating the viscosities at each shell, if the temperature was below T_{crit} , the solidus viscosity equation was used, and for higher temperatures, the liquidus viscosity equation, in equation [15](#).

Table 2: Table of constants for calculating the viscosity of the rocky core.

Term	Symbol	Unit	Value
Viscosity of solids at solidus	η_s	Pa·s	10^{18}
Viscosity of melt at liquidus	η_l	Pa s	0.1
Diffusion creep constant	α_η		26
Maximum packing crystal fraction	ϕ_m		0.64
Temperature of solids at solidus	T_{sol}	K	1425
Temperature of melt at liquidus	T_{liq}	K	1850

2.2 Radius of a hydrated rocky core

In the numerical model for core evolution the most important parameter is the initial radius of the hydrated rocky core. For most moons simulated the total radius, total mass and silicate mass (M_{sil}) were given in [Husmann et al. \(2015\)](#), however due to the initial core being hydrated, the total *core* mass, and the initial radius must be adjusted to account for the density of hydrated silicates.

Since the hydrated core consists most abundantly of antigorite, which is a serpentine ([Castillo-Rogez and Lunine, 2010](#)), it consists of 13%wt water. Knowing this we can say that the total mass of the hydrated core is expressed by $M_{\text{core}} = M_{\text{sil}} + 0.13M_{\text{core}}$, giving $M_{\text{core}} = M_{\text{sil}}/0.87$. Thus, using the density of hydrated silicates from table [1](#)

to express the volume of the core as

$$V_{\text{core}} = \frac{4}{3}\pi R_{\text{core}}^3 \equiv \frac{M_{\text{sil}}}{0.87\rho_{\text{hy}}},$$

we can find the radius of a hydrated core from the given silicate mass as

$$R_{\text{core}} = \left(\frac{3}{4\pi} \cdot \frac{M_{\text{sil}}}{0.87\rho_{\text{hy}}} \right)^{1/3}. \quad (16)$$

In the case of Mimas, the initial hydrated core radius was calculated from the total mass, total radius and mean density, M_{total} , R_{total} and $\bar{\rho}$ respectively, from a system of equations,

$$\begin{cases} M_{\text{total}} &= \rho_{\text{ice}}V_{\text{ice}} + \rho_{\text{core}}V_{\text{core}} \\ \bar{\rho} &= \frac{M_{\text{total}}}{V_{\text{ice}}+V_{\text{core}}}, \end{cases} \quad (17)$$

where ρ_{core} is the density of a hydrated core. The core radius is thus found as

$$R_{\text{core}} = \left(\frac{3}{4\pi} \cdot \frac{M_{\text{total}} - \rho_{\text{ice}}V_{\text{ice}}}{\rho_{\text{core}}} \right)^{1/3}, \quad V_{\text{ice}} = \frac{M_{\text{total}} \cdot \rho_{\text{core}}}{\bar{\rho}(\rho_{\text{core}} - \rho_{\text{ice}})} - \frac{M_{\text{total}}}{\rho_{\text{core}} - \rho_{\text{ice}}}. \quad (18)$$

Table 3: Radii of the hydrated rocky cores of all moons considered in this work with references to the constants used to calculate them.

Moon	R_{core} (km)	Source
Titan	2123.94	Hussmann et al. (2015)
Rhea	407.19	Hussmann et al. (2015)
Mimas	91.04	Schubert et al. (2007)
Io	2134.58	Hussmann et al. (2015)
Europa	1693.34	Hussmann et al. (2015)
Ganymede	2219.21	Hussmann et al. (2015)
Callisto	1952.44	Hussmann et al. (2015)

2.3 Analytical model for core evolution

The analytical model used here was first defined in Carslaw and Jaeger (1959) and recreated here following Elkins-Tanton et al. (2011) and compared to the results of Hevey and Sanders (2006). It is the solution to the differential equation of heat transfer by conduction in a sphere where a single radiogenic element is evenly distributed. It is only valid for a constant thermal diffusivity and a single element as a radiogenic heat source, motivating the use of a numerical model to facilitate several radiogenic elements in this work. They defined the temperature T of a planetesimal with a total radius R at a subradius r at time t since formation, taking into account only the

radiogenic heating from one element, ^{26}Al . This is defined analytically as

$$T = T_0 + \frac{\kappa A_0}{K\lambda} e^{-\lambda t} \left[\frac{R \sin \left[r \left(\frac{\lambda}{\kappa} \right)^{\frac{1}{2}} \right]}{r \sin \left[R \left(\frac{\lambda}{\kappa} \right)^{\frac{1}{2}} \right]} - 1 \right] + \frac{2R^3 A_0}{r\pi^3 K} \sum_{n=1}^{\infty} \frac{(-1)^n}{n \left(n^2 - \frac{\lambda R^2}{\kappa \pi^2} \right)} \sin \left(\frac{n\pi r}{R} \right) e^{-\frac{\kappa n^2 \pi^2 t}{R^2}}, \quad (19)$$

in [Elkins-Tanton et al. \(2011\)](#), where constants from [Hevey and Sanders \(2006\)](#) were used as defined in table [4](#). Initially the temperature is throughout the planetesimal at $T_0 = 300\text{K}$.

Table 4: The values of constants used in equation [19](#)

Term	Symbol	Unit	Value
Surface temperature	T_0	K	250
Thermal diffusivity	κ	$\text{m}^2 \text{s}^{-1}$	$7.6 \cdot 10^{-7}$
Initial power per unit volume	A_0	W m^{-3}	$6.4 \cdot 10^{-4}$
Thermal conductivity	K	$\text{W m}^{-1}\text{K}^{-1}$	2.1
Decay constant	λ	s^{-1}	$3.01 \cdot 10^{-14}$
Total radius	R	km	50

2.4 Simulating convection in the rocky core

The onset of convection in any body is most easily tracked using the Rayleigh number, defined in equation [14](#). If the Rayleigh number surpasses a critical value of $Ra_{\text{crit}} = 10^3$ then the shell can be considered mainly convective. The exact ratio of convective to conductive heat flow in a shell is given by the Nusselt number, defined as $Nu = (Ra/Ra_{\text{crit}})^{0.25}$ where $Ra > Ra_{\text{crit}}$ ([Desch et al., 2009](#)). Simulating convection is of particular importance since it is a more efficient method of heat transport than conduction.

Similarly to [Desch et al. \(2009\)](#) the convection in the rocky core in this work is simulated by adjusting the conductivity in areas that surpass Ra_{crit} to the effective conductivity as follows. The effective conductivity is defined as $k_{\text{conv}} = k \cdot Nu$ where the Nusselt number is dependent on the intrinsic conductivity. The issue with higher effective conductivities is that they imply very short time steps, which would slow down the simulations far too much to be efficient. This is addressed by assuming a fixed value for the Nusselt number used to calculate the effective conductivity, varying it from 10^1 or 10^2 to 10^3 when comparing the effect of the assumed Nusselt number's value but otherwise when simulating moons that become unstable to convection, the assumed Nusselt number is set to $Nu = 100$.

3 Results

In this chapter the results of all described simulation models are given. Initially the correctness of the implementation of the numerical model was checked by comparing to the analytical model for temperature evolution in a core heated by a single radioactive element. This is followed by the results of numerical simulations of the rocky cores of Saturn’s moons Rhea, Mimas and Titan, showing how the sizes of the different cores affect the temperature and processes occurring in them. Finally, Jupiter’s moon Europa is also simulated and an analysis of the effects of different remaining potassium fractions is presented.

3.1 Analytical model

In order to determine that the analytical model was correctly implemented, a simulation was run with the exact same parameters as used in figure 1a of [Hevey and Sanders \(2006\)](#). The object simulated was a rocky planetesimal with a radius of 50 km divided into 50 shells, a constant time step of 1041.5 years, and a surface temperature of 250 K, heated only by ^{26}Al , with the other thermal constants given in table [4](#). The analytical results along with a numerical simulation with the same parameters is recreated in figure [5](#) here.

The general trends seen in a rocky core include a small radial temperature difference apart from the differences stemming from energy loss through the surface, and a temperature profile of initial exponential growth followed by cooling as seen in figure [5](#) (a).

Initially the two models differ significantly due to the temperature gradient between layers being extremely small and the spatial resolution of the numerical model not being high enough to account for that. This was determined by the thickness of a shell being greater than the thickness of the thermal boundary layer between the uniformly heating core and the constant surface temperature giving $\sim \sqrt{\kappa t} = 158 \text{ m}$ ([Kirk and Stevenson, 1987](#)). Since the thickness of a shell used was $50 \text{ km}/50 = 1 \text{ km}$ and the thermal boundary layer remained smaller than that for the first 41 000 years of the numerical simulation, the two models are significantly different in the beginning of the simulation.

Since the analytical model only allows for heating from a single radiogenic element, the comparisons of the numerical and analytical models were also made for each of the elements used in the numerical model, namely ^{40}K , ^{235}U , ^{238}U and ^{232}Th , though only the comparison with ^{26}Al is shown here in figure [5](#). The parameters for these elements were taken from [Desch et al. \(2009\)](#) and as can be seen in figure [5](#) (b), representing heating from only ^{26}Al . The differences between the analytical and numerical models do not exceed proportions greater than 10% here, including the initial differences, as was the case for the other elements.

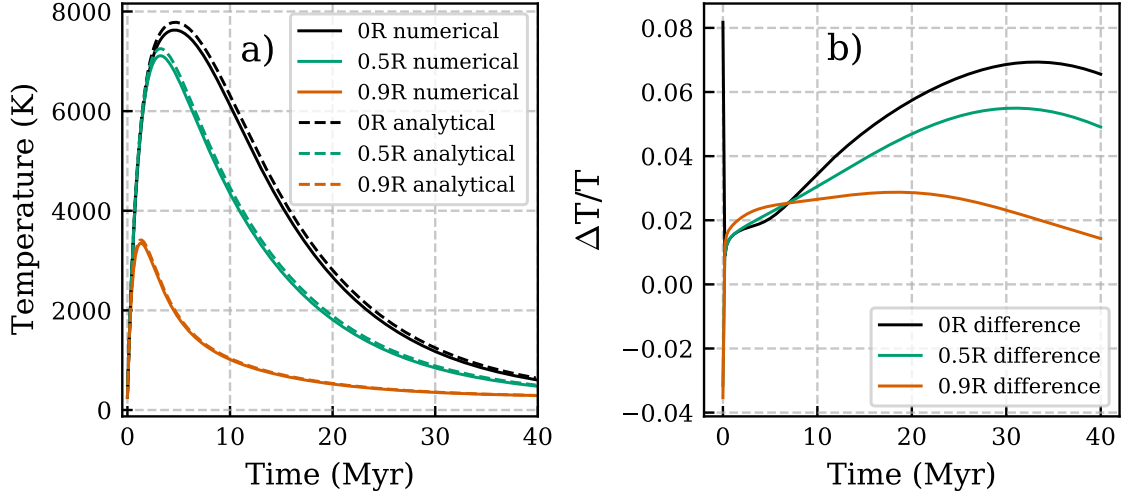


Figure 5: The differences between the numerical and analytical model for an object with the same parameters and heated only by ^{26}Al , at the centre ($0R$), halfway to the surface ($0.5R$) and near the surface at $0.9R$. (a) shows the recreated analytical solution from [Hevey and Sanders \(2006\)](#) in dashed lines overplotted with the numerical solution in solid lines. (b) shows the fractional difference between the models.

3.2 Rhea and Mimas

The surface temperature of the rocky cores of moons were set to a constant 300K until it can be coupled with a model for the ice mantle on top of it. This temperature was chosen following [Castillo-Rogez and Lunine \(2010\)](#). It is important to note that for the standard simulations of all moons the potassium leaching was set to 70%, leaving 30% of the initial potassium to heat the core.

Rhea and Mimas are two moons of Saturn, chosen for simulating to show how core sizes affect the results. Since these two moons have cores that are rather small, the temperature increase from the radiogenic heating quickly becomes overwhelmed by the low surface temperature, ensuring that the cores of these moons never dehydrate. This effect is more apparent the smaller the moon in question is, and can be understood when comparing cooling through the surface to the equation of heating (equation [1](#)). Heating $Q \propto R^3$ and cooling is $\propto R^2$ since heat is only lost through the surface. Thus, the ratio of cooling to heating is proportional to $1/R$, causing a sharp difference in heating and thus temperatures reached, depending on the total radius of the object.

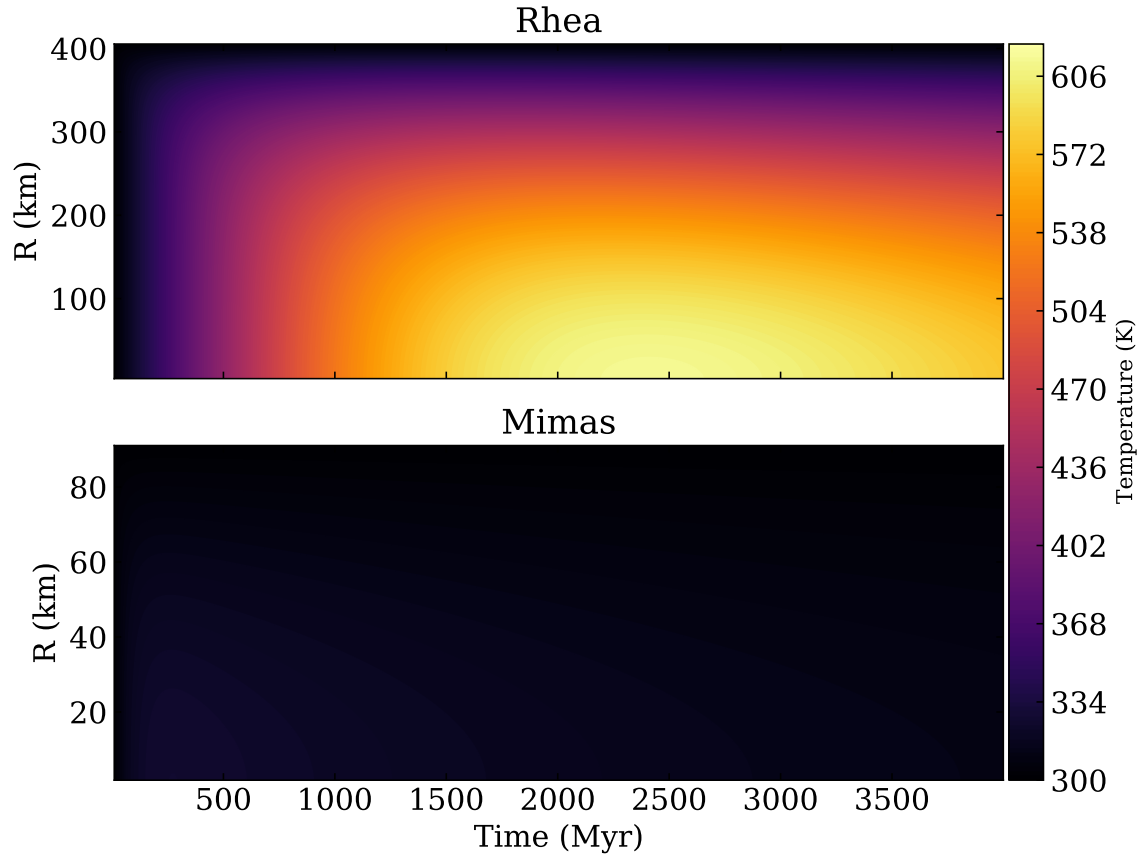


Figure 6: The temperature evolution in colour for Saturn’s moons Rhea and Mimas, exemplifying the difference in temperatures reached, depending on the core radii.

In figure 6 the temperature evolution in colour is given over time (x-axis) at all radii (y axis) for the cores of Rhea and Mimas with 30% of original potassium remaining in the cores. Here the profound difference in temperatures reached over $4 \cdot 10^9$ years becomes apparent, having chosen the same temperature range in colour for both cores to exemplify just that. While Rhea continuously heats up until a maximum central temperature is reached at about 2500 Myr, Mimas manages to heat only initially, reaching its maximum central temperature at 250 Myr, before being overwhelmed by the heat loss through the surface.

3.3 Titan

Titan has a core radius greater than 2000 km, hence it reaches very high temperatures and can go through the process of dehydration. Here the simulation on Titan is run with 30% of the original potassium-40 assumed to remain in the core.

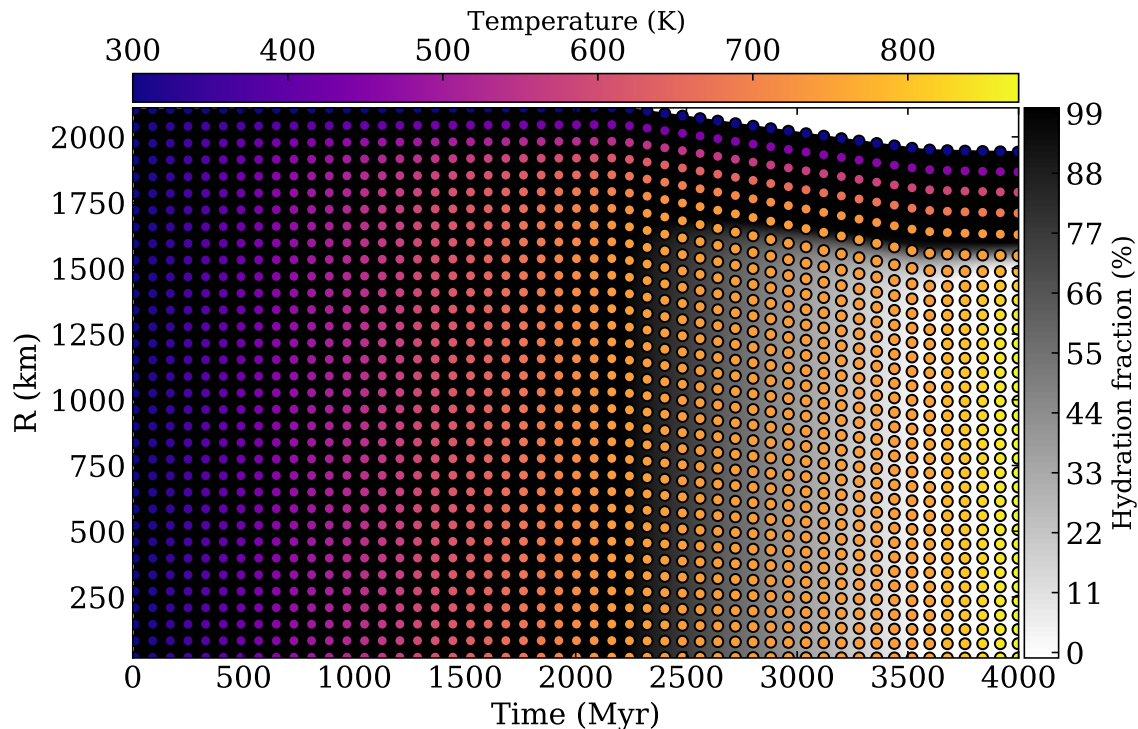


Figure 7: Titan’s thermal evolution in coloured dots with the hydration fraction shown in grayscale.

In figure 7 the thermal evolution and hydration fraction of Titan’s silicates are over-plotted to show their dependence on one another. The temperature evolution is given in coloured dots and the hydration fraction in the grayscale background, which is initially fully hydrated in black and transitions to white in areas where dehydration occurs, simultaneously with the core radius decreasing. Since dehydration is an endothermic reaction, it claims all the energy created radiogenically until the process is complete, keeping the temperature constant until dehydration is complete. Since this is the most likely simulation of Titan’s core to resemble reality with the 30% remaining K (Castillo-Rogez and Lunine, 2010), the temperature would still be increasing to this day, according to this model.

During dehydration the core of the moon shrinks as the water that is separated from the silicates is assumed to be transported immediately to the ice mantle. This is particularly noticeable for Titan in figure 7 as over three quarters of the core radius becomes dehydrated.

Another simulation was run for Titan to determine the maximum possible temperature that Titan’s core can reach up to present day. To this end a simulation was run assuming no potassium leaching, thus keeping the fraction of chondritic potassium at 100%. The results of this simulation are presented in figure 8 where the temperature of Titan’s core is shown as a function of radius and time. The greatest difference with the 30% remaining potassium model is that dehydration, indicated by the decrease

in core radius, occurs much more rapidly. Since the temperatures reached as seen in figure 8 are very high, a convective model was triggered with the assumed Nusselt number of $Nu = 100$. Here convection is triggered at roughly 2700 Myr and will be discussed further in section 3.5, along with melting and differentiation of a metallic core

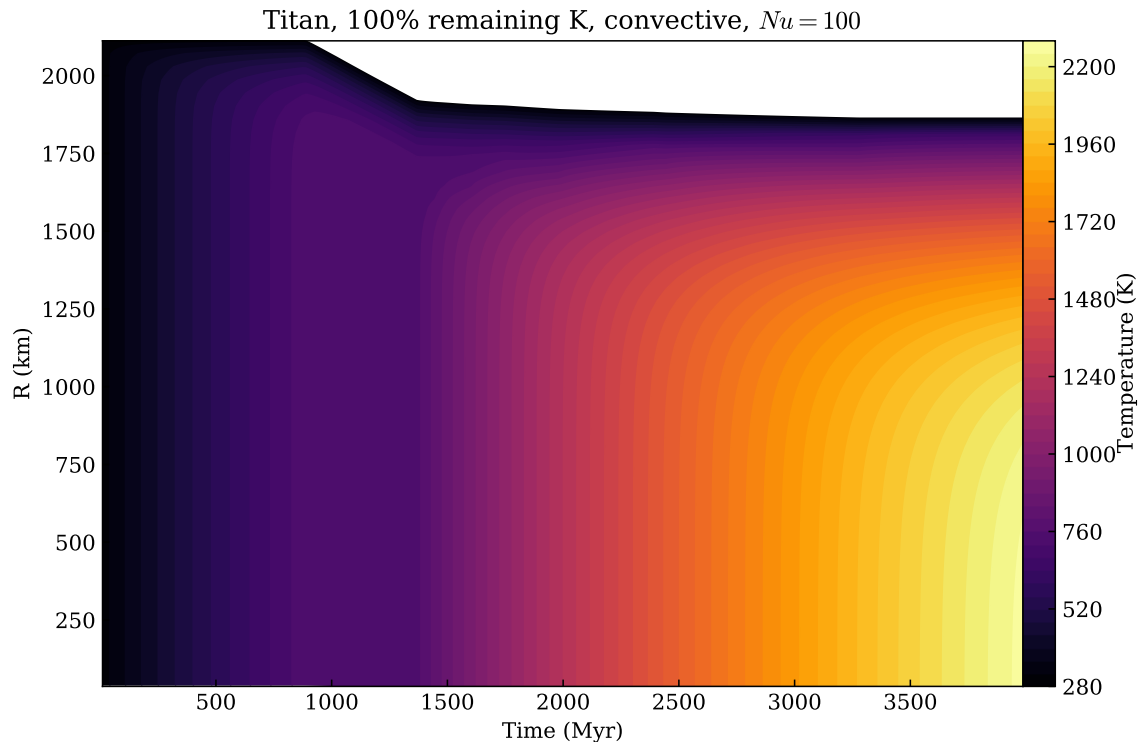


Figure 8: Titan’s thermal evolution in colour with 100% remaining potassium.

3.4 Europa

The most important parameter for running the simulation is the initial radius of a completely hydrated core, thus the choice of moon for simulating must be based on that. As can be seen from table 3, the fully hydrated core radii of the Galilean moons, apart from Europa, are similar to Titan’s. For this reason the simulation code is not run for Callisto, Io or Ganymede, rather choosing Europa with its core radius of 1693 km for comparing to cores with a similar radius.

In figure 9 the temperature evolution in coloured dots and hydration fraction in grayscale are given as functions of radius and time under the assumption of no potassium leaching. From figure 9 it is apparent that the slightly smaller core of Europa does not reach as high temperatures as Titan’s core before the present day at 4000 Myr, yet it still reaches temperatures high enough to begin convection if the remaining potassium fraction is high enough. The simulation itself was run for significantly longer than present day. The peak temperature of this simulation is reached at 6400

Myrs at a significantly convective stage.

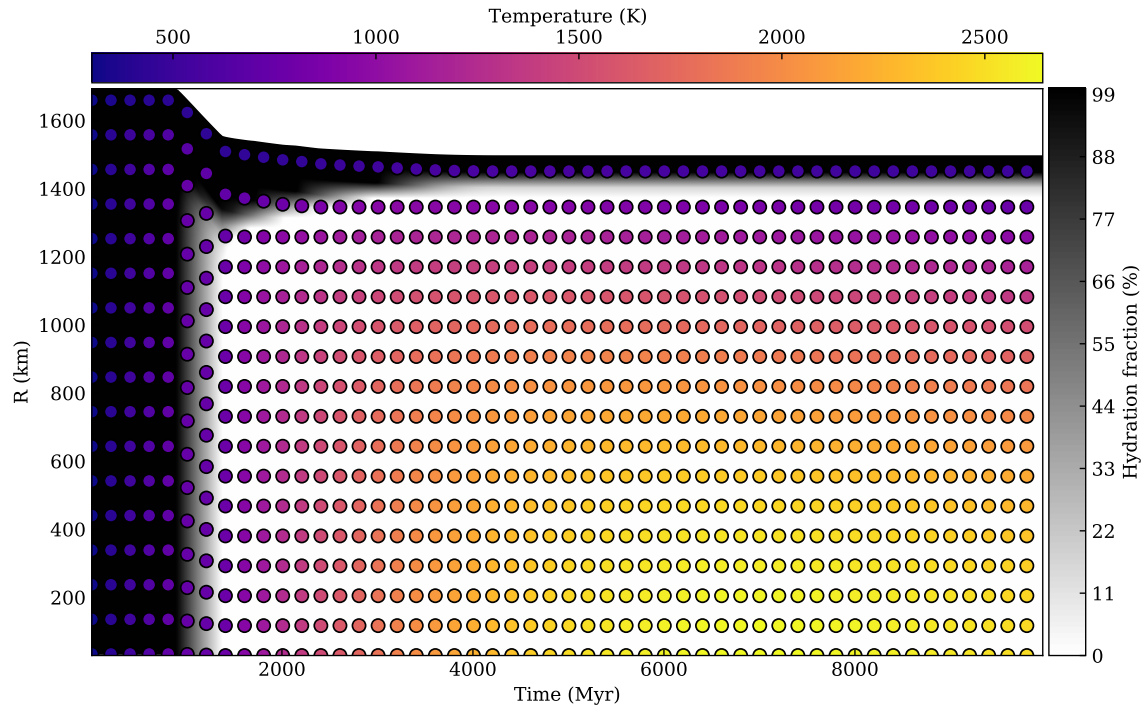


Figure 9: Europa's thermal evolution with 100% of the chondritic potassium remaining with the temperature in coloured dots and the hydration fraction in grayscale over a time period of 10 Gyr with the present day at 4 Gyr.

In figure [10](#) only the thermal evolution of Europa's core as a function of time and radius is given with the maximum 100% and the estimated 30% remaining potassium. Here the core temperatures are markedly different from each other. With the maximum potassium fraction present, Europa's core dehydrates very early, before 1500 Myrs, and reaches temperatures up to 2225 K in the centre by 4000 Myrs, making the presence of an ocean at present day very likely. In the lower plot with only 30% potassium remaining the temperature evolution is held up by dehydration from 2100 to 3600 Myrs, ending the dehydration process only a few hundred Myr before present day. This indicates that at any potassium fraction Europa's core is still heating at present day.

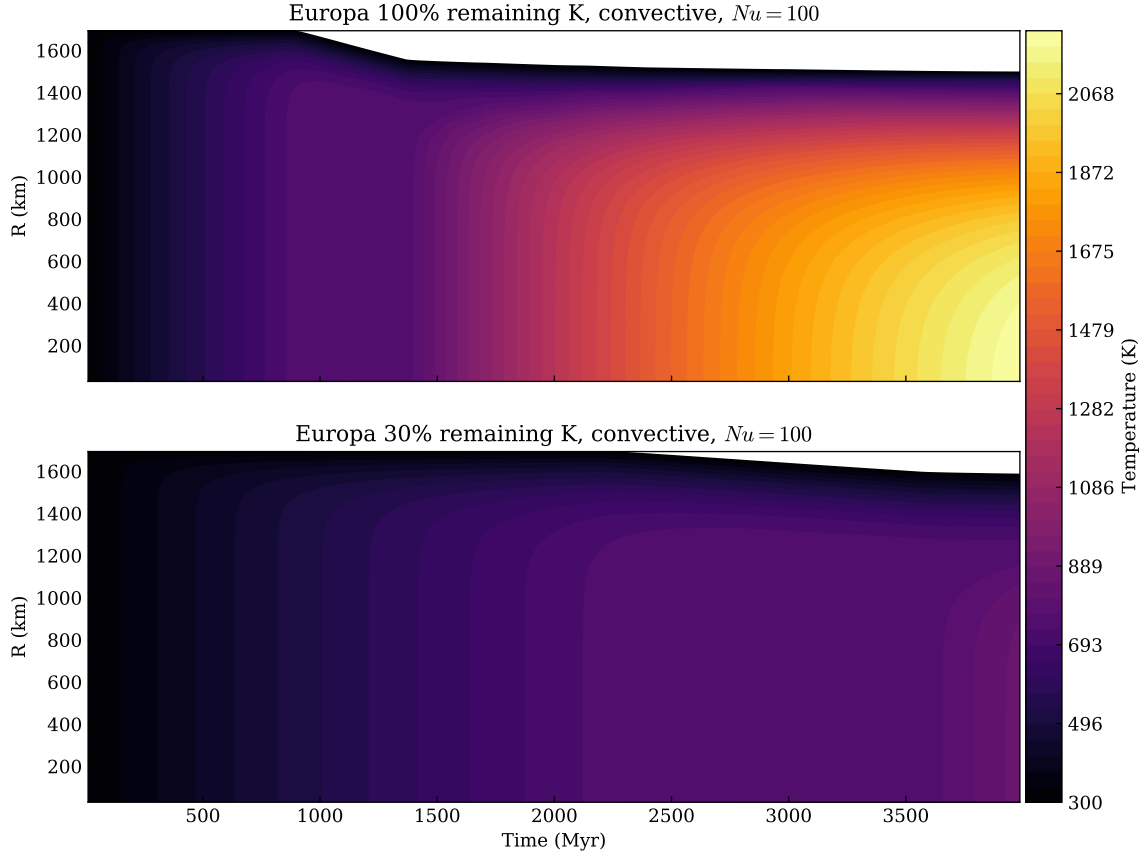


Figure 10: Europa’s thermal evolution in colour over a time period of 4 Gyr up to the present day with the plot above showing evolution with 100% of the chondritic potassium remaining in the core and the plot below with the estimated 30% potassium remaining. The temperature axis is joint for the two cases in order to emphasise the difference in temperature evolution.

3.5 Melting and convection of the core

At high enough temperatures it is possible for the silicates of the rocky core to decrease their viscosity and begin convecting or even melt entirely. As seen in previous sections this is most likely to occur within the largest moons of the Solar System, such as Titan. In this section the extent of possible convection in the largest moon investigated in this work, Titan, is presented. This is done by following the Nusselt number, which gives the ratio of convective to conductive heat transfer in every shell of the core where values of $Nu > 1$ can be considered convective. This is shown in figure 11 where the evolution of the Nusselt number is given in a logarithmic scale in colour as a function of time and radius, with the simulation run on Titan’s core with no potassium leaching for maximum temperatures. The Nusselt numbers reached are as high as 10^5 , which are much higher than the values assumed in the model, but implementing these in the numerical model would make the simulation unfeasably slow.

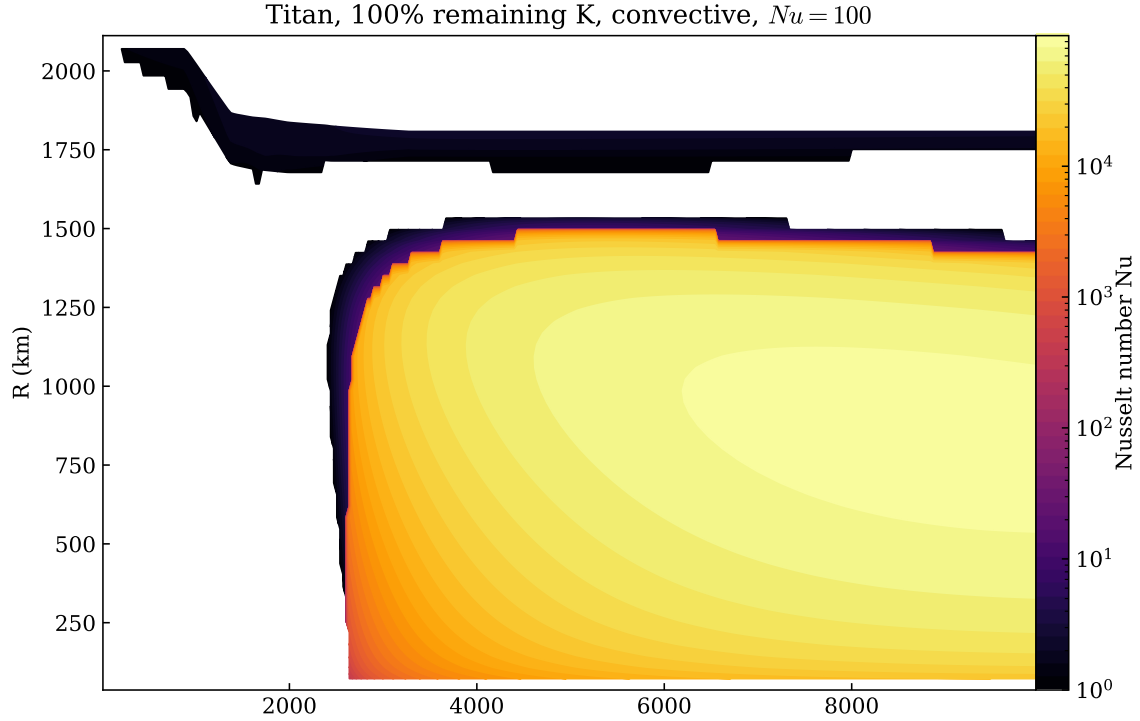


Figure 11: The evolution of Nusselt’s number in Titan’s core in colour over a time period of 10 Gyr with the core radius on the y-axis and the time passed on the x-axis. White areas in the figure where the Nusselt number is not given represent a purely conductive regime where $Ra < 1000$ and the Nusselt number is not calculated.

In a rocky core melting can only occur at very high temperatures and will then lead to the differentiation of metals from silicates, forming a metallic core. The melting of a rocky core can be tracked using the critical volume fraction of melted material ($\phi > 0.36$) defined in equation 15. In figure 12 the volume fraction of melted material at all radii over time is shown in a diverging colourmap with melted silicates shown in red and solids in blue. This is shown for the maximum, 70% and 30% of the possible remaining potassium for Titan, since it is the largest moon and thus most likely to reach high enough temperatures to melt.

In figure 12 it is clearly shown that melting of the rocky core is a very much possible occurrence, since all cases reach a value of $\phi = 1$, indicating a completely melted region. Surprisingly, it is possible for the rocky core to melt even at low remaining potassium fractions, it simply does not trigger before 6000 Myr, thus making melting and the differentiation of metals from silicates a future event.

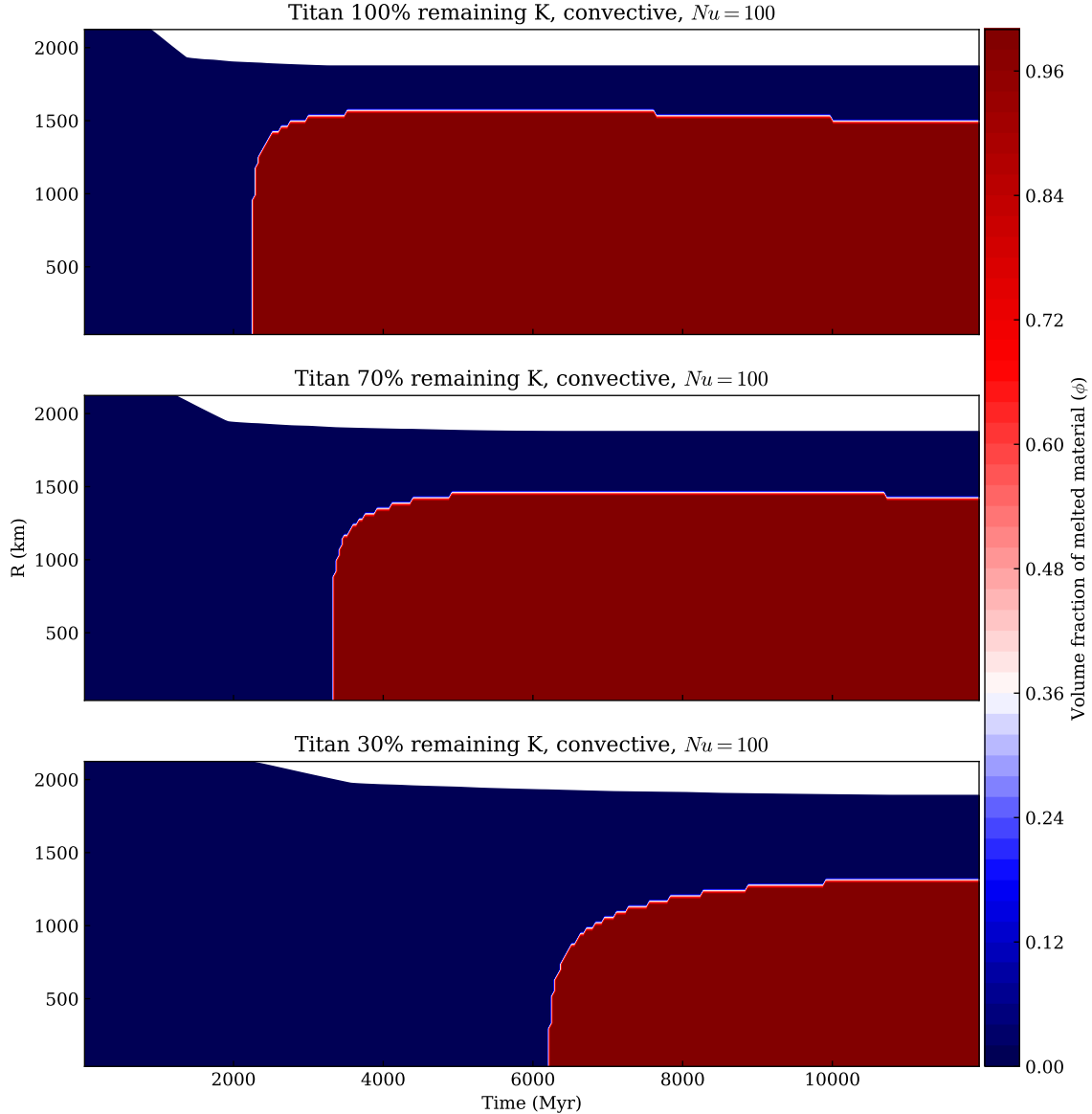


Figure 12: The evolution of the volume fraction of melt in Titan’s core in colour over a time period of 10 Gyr with the core radius on the y-axis and the time passed on the x-axis. Melting occurs when in the red regions while blue regions at lower temperatures are considered solid.

3.5.1 Differences in the conductive and convective models

The change in conductivity that a convective model imposes on a rocky core of a moon directly affects the efficiency of heat transport. Thus, it would be expected for a moon in the convective regime to cool more quickly than a purely conductive model at the same fraction of remaining potassium. In figure [13](#) the temperature difference between a conductive and convective case with the assumed Nusselt number of $Nu = 100$ is given over a time of 10 Gyr and as a function of both time and radius. From the

figure it is apparent that the temperature difference between the two models remains small for the values of the investigated Nusselt number.

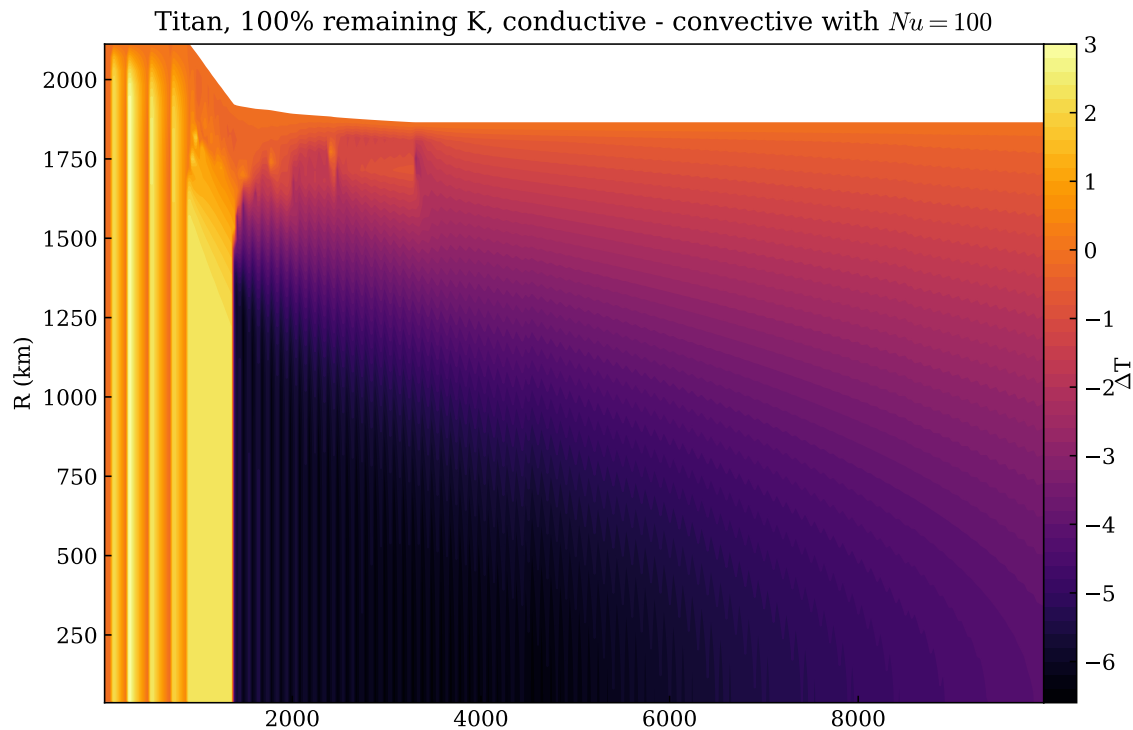


Figure 13: Titan’s core’s evolution over 10 Gyr, showing the temperature difference between the conductive and convective models in colour.

In figure 13 the dehydration process happens early, indicated by the decrease in core radius. Immediately afterwards, when temperatures are allowed to rise again, the convective regime soon begins to dominate, with the temperature difference between two regimes indicated by the switch to negative values.

3.6 Onset of cooling in the rocky core

When searching for conditions for life in the form of a liquid ocean it is also important for the ocean to be sustained over a long period of time. For this reason it would be good to know roughly when the cores of large icy moons begin to cool. For this purpose Titan’s core was simulated over a very long time period of 12 Gyr and comparing three different remaining potassium fractions. The potassium fractions used were 100%, 70% and 30% to show the most extreme case, the case in which convection is very likely to occur at some point in time and the case that is most likely with the lowest simulated potassium fraction. In figure 14 the temperature evolution as a function of radius is shown for the three described cases, with a joint colour bar to show the differences between the temperature evolution tracks.

From figure 14 it is clear that the lower the fraction of remaining potassium in the

core the lower the maximum temperatures reached are and the later the core begins to cool. At the present time of 4000 Myr from the beginning of the simulation, Titan's core is not cooling at any fraction of remaining potassium.

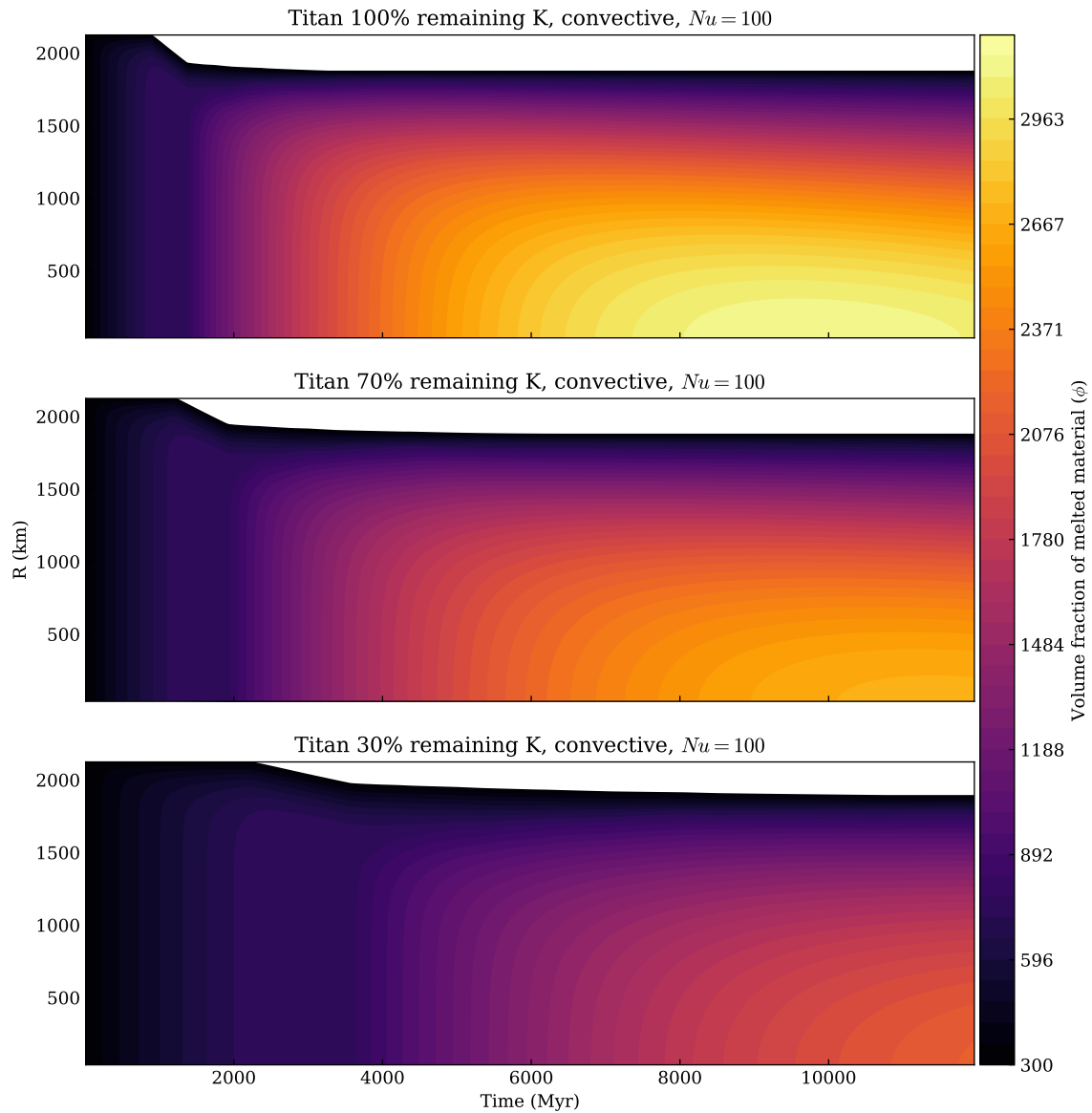


Figure 14: Titan's core's evolution over 12 Gyr for different remaining potassium fractions, showing the temperature in colour.

4 Discussion

4.1 Limitations of a purely conductive core model

A purely conductive numerical model for the rocky core is correct as long as the primary method of heat transport is conduction. For this reason several runs were made with Titan’s core to determine roughly at what conditions the temperatures become high enough for the melt fraction to become significant enough for a convective model to become necessary to preserve accuracy. The model was deemed to be inaccurate if at any point the Rayleigh number became greater than 10^3 . As can be seen in figure 15 the core becomes unstable to convection only if the potassium leaching fraction has been very small, reaching temperatures greater than the critical temperature of 1637.5 K at which a liquid viscosity equation must be used.

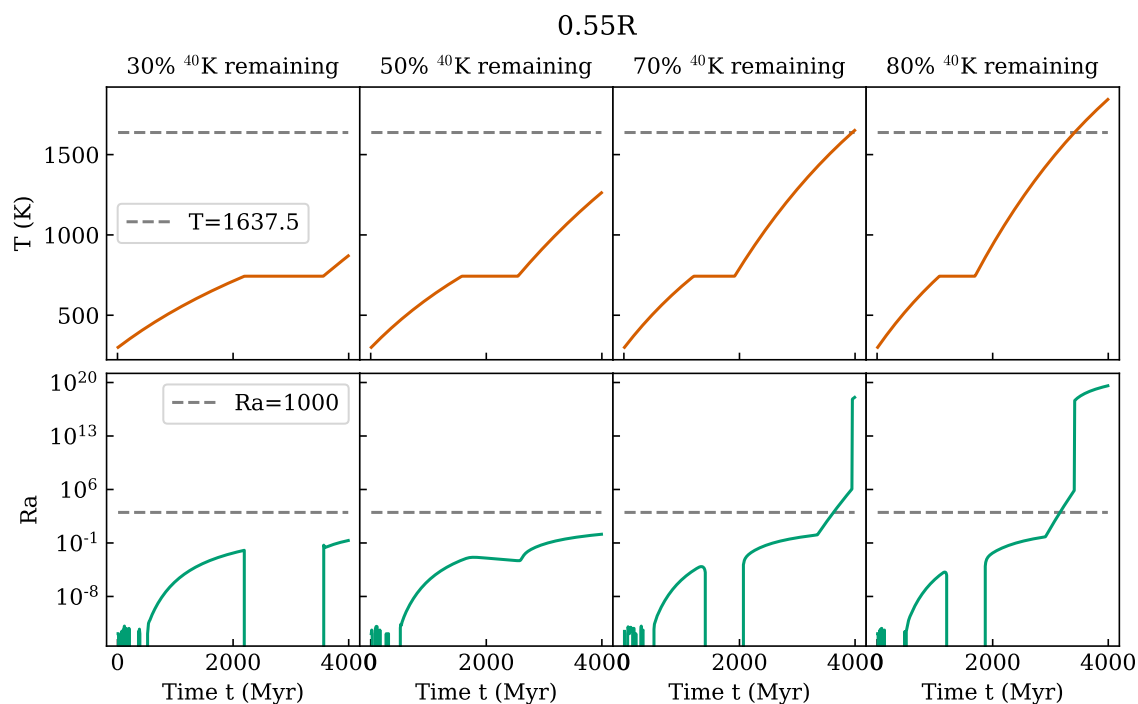


Figure 15: The evolution of Titan’s temperature and Rayleigh number for four different potassium leaching fractions, leaving, from left to right, 30, 50, 70 and 80% of the original potassium remaining. In the temperature plots (top row) the critical temperature is shown in a dashed line, above which the formula for viscosity (equation 15) must be changed to a liquid one. In the Rayleigh number plots (bottom row) the critical value of 1000, above which the conductive model becomes inaccurate, is shown as a dashed line.

The reason why the temperatures and Rayleigh numbers over time have been shown not in the centre of the core, but at $r = 0.55R$, is that this shell reaches roughly the highest Rayleigh numbers. This is so because in the inner $\sim 80\%$ of the core radius

the temperature gradient is small and the radial changes in the Rayleigh number are dominated by gravity, which is greatest further from the centre. At radii greater than $0.55R$ the Rayleigh number begins to decrease due to the lower temperatures from heat loss through the surface.

In all figures the Rayleigh number is initially unstable as the temperatures are low and the Rayleigh number is dominated by numerical noise. As the temperature increases over time and decreases viscosity, the Rayleigh number also increases, apart from the duration of dehydration (indicated by a constant temperature), during which the lack of a temperature gradient between shells significantly decreases the Rayleigh number.

In the two Rayleigh number plots with the greatest remaining potassium fractions there are several transitions in the curve. The first of them, right before reaching the critical Rayleigh number, comes from the rapid decrease in viscosity at that time, due to the first appearances of silicate melt. The second transition, occurring after reaching Ra_{crit} and initiating a near vertical growth, coincides with the shell reaching the temperature at which viscosity formulas are switched.

4.2 Comparison of the convective and conductive model

As is apparent from figure [13](#), the resulting temperature evolution in a simulation does not differ much between a fully conductive and a convection-considering model. This is likely due to the rudimentary nature of the current convection model, which simulates a convection that is not as efficient as it would be in reality. In reality one would expect a convecting moon to cool much more efficiently than a conductive one, though that would affect the accuracy of this model at a very late simulation time, since cooling, as is apparent from figure [14](#), does not take place before present times. Thus, it can be said that the code written in this project is moderately reliable until temperatures in a convecting moon begin to drop.

4.3 Effects of potassium leaching

As is apparent from figure [15](#), different fractions of remaining chondritic potassium after leaching, lead to greatly different temperatures reached in the rocky core. Since it is difficult to accurately estimate the actual potassium leaching fraction, this leaves a large uncertainty in temperatures reached in the core, and possibly also the formation and endurance of a liquid ocean.

Another process that potassium leaching may affect is the possible differentiation of metals from silicates if the temperatures become high enough for the metals to melt and percolate to the centre of the core ([Néri et al., 2019](#)). The differentiation of metals from silicates would take place at the extremely high temperatures reached in the core if the potassium leaching fraction were especially small, possibly allowing for a partial or even full differentiation between metals and silicates.

Also, the time it takes for dehydration varies strongly with the remaining potassium fraction, with the process taking place significantly earlier for higher values. Additionally, for higher remaining potassium fractions the duration of dehydration is significantly decreased, as can be seen from the varying lengths of constant temperature in figure [15](#).

4.4 Assumed and actual Nusselt number

The Nusselt numbers used for calculating an effective thermal conductivity in order to simulate convection were assumed to be either 10, 100 or 1000, hence the actual Nusselt numbers defined in section [2.4](#) at every time step should be compared to it, to assess the validity of those assumptions. In figure [11](#) where Titan's maximum possible Nusselt number is shown, it can reach values up to 10^5 which is significantly greater than the assumed value of $Nu = 100$ used for all simulations where convection was a possibility. However, if the assumed Nusselt number were raised to such a high value it would make the variable time step calculated by the Courant condition far too small to retain the efficiency of the code, making the simulation run too slow to be practical.

It should also be emphasised that the difference between runs of convective simulations with different assumed Nusselt numbers were negligible, confirming that the choice of assumed Nusselt number does not have a significant impact on the results.

4.5 Effect of time step length and number of shells on results

In order to determine whether the choice of percentage of the Courant condition for the stability of the simulation affects the results, a long simulation is not needed. Therefore, for this purpose the core of Titan with 30% of original potassium remaining was simulated until 300 Myr with a variable time step chosen as 1%, 5% and 10% of the calculated Courant stability condition.

As can be seen from figure [16](#) where the temperature difference is given for different Courant conditions used, the greatest differences only occur at the beginning of the simulation. This is likely due to the simulation relaxing to the initial conditions, since the very low initial temperature gradient cannot be resolved until some temperature evolution occurs. Therefore, the choice of the percent of minimal timestep that the Courant stability condition gives, does not have much of an effect on the simulation after the initial relaxation ceases.

Similarly to the comparison of different Courant condition percentages, a comparison of the results with different numbers of shells used was run with the same parameters other than a slightly longer simulation time of 500 Myr. The results of this comparison are seen in figure [17](#) where again, initially the differences in temperature are great due to relaxing to initial conditions, but the difference in temperature disappears entirely, showing that within reason the choice of shell number does not affect the results much.

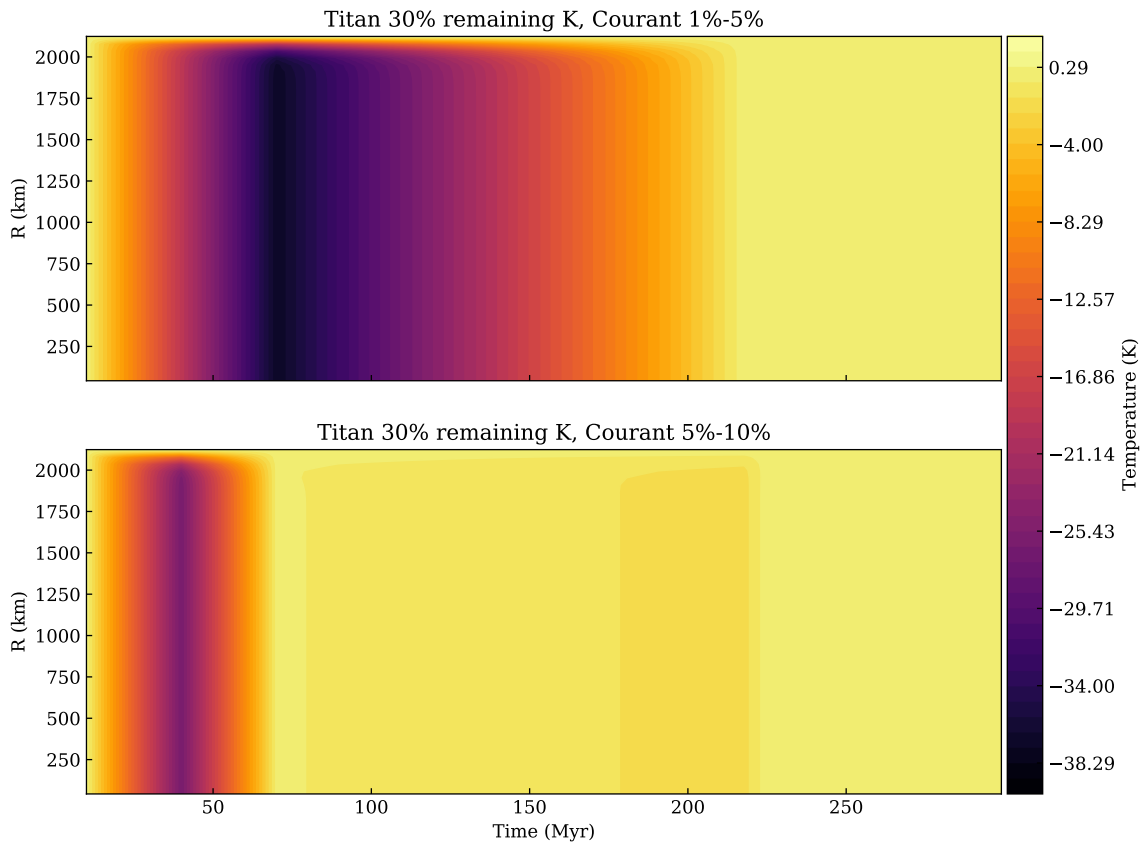


Figure 16: The temperature difference when using Courant stability conditions of 1% - 5% and 5% - 10% as exemplified by the first 300 Myrs of Titan's evolution with 30% of chondritic potassium remaining.

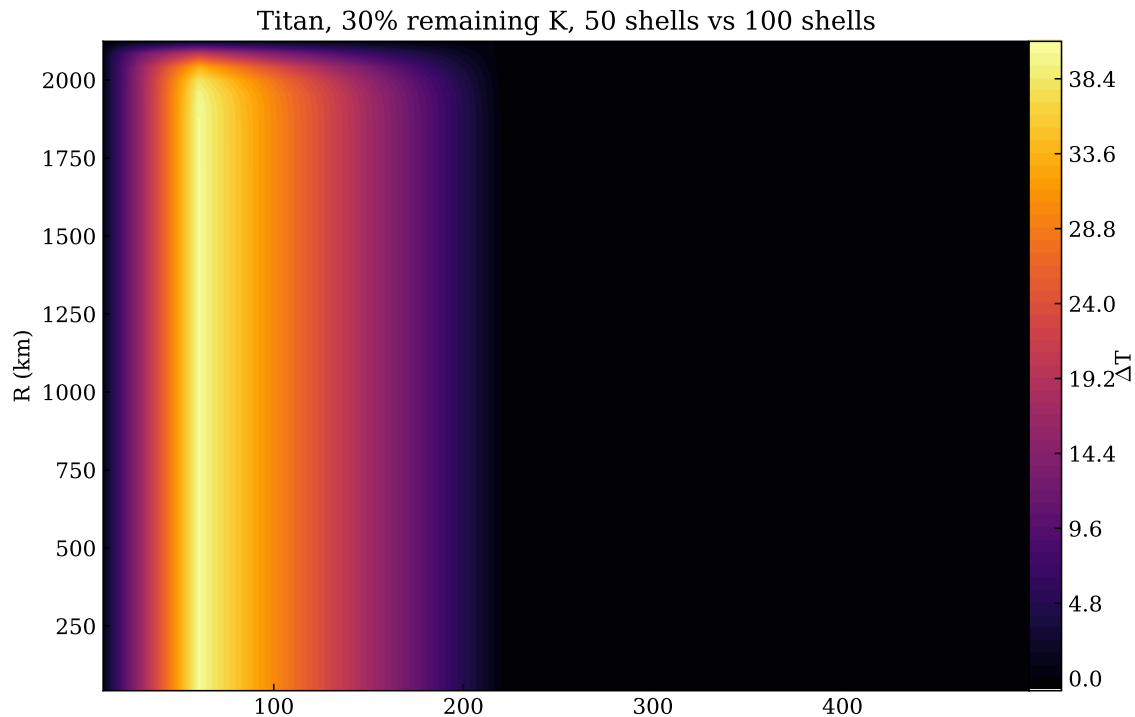


Figure 17: The temperature difference when a simulation is run with 50 shells and 100 shells as exemplified by the first 500 Myrs of Titan’s evolution with 30% of chondritic potassium remaining.

4.6 Other heating mechanisms

The most important heating mechanisms that are not modelled in this work are tidal and gravitational heating. Tidal heating would be most significant for Io, and to a lesser extent also for Ganymede and Europa. Gravitational heating should most importantly be considered for moons where temperatures become high enough to initiate melting and subsequent differentiation of metals from the silicates of the core. Thus, gravitational heating is most important secondary heating method to consider firstly in moons, where the fraction of remaining potassium in the silicates is extremely high and also that have a silicate core large enough to facilitate such unopposed temperature growth. Since the fraction of remaining potassium in any silicate core is a subject of debate, no specific moons can be named as most enriched in potassium, and therefore most efficiently heated.

Of the moons considered in this thesis the highest temperatures at the same remaining chondritic potassium remaining, are reached in the ones with the largest cores, namely Titan and those with similar core radii, found in table 3 and namely Io, Ganymede and Callisto.

5 Future developments

A model for simulating the entire large icy moon, complete with the ice mantle and its numerous processes, is already in the works. This chapter gives an overview of many possible expansions to associate with this model of the rocky cores of large icy moons.

The ice mantle is a complex model to create because of several factors, most importantly because a large portion of the water-ice phase diagram must be considered for an accurate model, complete with the possible formation of high pressure ices. Modelling an ice mantle requires the calculation of a surface temperature to be found by the assumption of thermal equilibrium. Internal heating of the ice mantle, which is yet to be modelled in existing literature, will also be considered. A very interesting addition to the current model would be a model for differentiation and setting the initial temperature array at different shells by existing formation models, for an even more realistic outcome.

5.1 Surface temperature

The surface temperature of any moon would be defined by the assumption of thermal equilibrium, with the energy emitted being equal to the energy absorbed from solar radiation reaching the moon's surface. The heat emitted by the moon would be defined by the blackbody radiation law as $Q_{\text{gen}} = 4 \cdot \pi R^2 \sigma T_{\text{surf}}^4$, where R is the total radius, σ is the Stefan-Boltzmann constant and T_{surf} is the unknown surface temperature. The heat from the sun is defined as

$$Q_{\odot} = (1 - A_b) \frac{L_{\odot}}{4\pi r_{\odot}^2} \pi R^2, \quad (20)$$

where A_b is the albedo of the moon, L_{\odot} the luminosity of the Sun, r_{\odot} the distance from the Sun to the moon, set to a constant value of the host planet's orbital radius, and R the radius of the moon itself. Now expressing T_{surf} from the blackbody radiation law and replacing in $Q_{\text{gen}} = Q_{\text{in}} + Q_{\odot}$, where Q_{in} is the total heat gained by the moon, we get

$$\begin{aligned} T_{\text{surf}} &= \left(\frac{Q_{\text{gen}}}{4 \cdot \pi R^2 \sigma} \right)^{\frac{1}{4}} = \\ &= \left(\frac{Q_{\text{in}}}{4\pi R^2 \sigma} + \frac{(1 - A_b)L_{\odot}}{16\pi r_{\odot}^2 \sigma} \right)^{\frac{1}{4}} \end{aligned} \quad (21)$$

as the surface temperature of any moon. In this equation the heat received by solar radiation affects the resulting surface temperature the most. For example Titan's surface temperature is calculated to be at an almost constant 82.3 kelvins over an extended time period, which is a similar value to the static 80K used in [Castillo-Rogez and Lunine \(2010\)](#).

5.2 Ice phases

One of the issues accompanying an ice mantle is addressing the different ice phases which depend on the temperatures and the temperature dependent pressures via the phase of the ice above. A pertinent simplification would be to band together the high pressure ices, allowing for only three phase distinctions of ice I, HP ices and liquid. This still encompasses three different phases with varying pressure-dependent densities, making the calculation of the total volume, therefore the total radius, complicated. One way to calculate the total volume would be to keep the densities phase-specific but that would require a recursive search for the exact pressure and temperature of the phase change, in order to both account for the phases and therefore pressures of the shells above but also preserve the total mass of the moon. This, in turn, gives an exact phase change radius from the pressure, giving the volumes of each phase, therefore the total volume, from which the total radius can be determined.

It is apparent from the phase diagram of ice (figure 1) that the temperature required for a liquid or near-liquid phase is not very high, compared to silicates. For this reason it is important to consider the structure of the ice mantle as it is likely to become unstable to convection at some point in time. As is described by Spohn and Schubert (2003), the ice mantle, once with a low enough viscosity to convect in places, consist of a stagnant, purely conductive lid, which sits on top of a convective layer, under which there may be an ocean. In addition, if high-pressure ices are considered, it is possible to have a layer of high pressure ices between the ocean and rocky core.

In the stagnant lid the temperature increases rapidly with depth, as heat is only transferred through conduction from the convective layer below. Due to the likely low viscosity of the ice mantle thanks to both the heating from the core below and internal heating from leached potassium, the mantle is believed to be mostly convective. Within the convective layer the change in temperature is expected to be small and follow an adiabatic structure with radius (Solomatov, 2007). If a liquid ocean occurs then it is expected to have the same temperature gradient. In the case of a high pressure ice layer existing, it would in turn consist of a similar stagnant lid and convective layer below, though with no ocean underneath it. The most important parameters in determining the temperature across the ice mantle are the surface temperature and the flux of heat from the rocky core below, in addition to the internal heating by potassium-40.

5.3 Internal heating of the ice mantle

The ice is likely heated very similarly to the rocky core, having leached at least some potassium from the rocky core in the early stages of the moon's lifetime. For this reason the internal heating model of the rocky core must be extended to the ice mantle as well. The water that is ejected from the core during dehydration does not contain the primitively leached potassium, therefore the fraction of primitive potassium in the convective regions must be tracked as the potassium-free water will mix with the

enriched water and ice.

All previous models for the ice layer of icy moons in the literature assume that the only source of heat in an icy moon is the radiogenic heat generated in the rocky core. This would be inaccurate if a significant amount of potassium is leached into the water in the early stages of the moon’s lifetime, which is likely, as discussed in section 4.3. In the extension of this work which is in progress, it is planned to also account for the heat generated by the potassium within the ice mantle itself, following the convection models of Vilella et al. (2018). However, with the convection model described in Vilella et al. (2018) being silicate-specific, it must be adjusted for ice instead, which has not been done before.

5.4 Core–mantle boundary

Another issue in modelling the core and mantle simultaneously is tracking the presence of an ocean at the core–mantle boundary since the dehydration-ejected water would mix with the potassium enriched water due to convection that is the main mode of heat transport in a liquid. For a model containing both the core and ice mantle the shells would be defined by radii with a constant ΔR since tracking the same silicate mass is no longer important. This introduces the issue of a shell containing both silicates from the core and some of the ice mantle sitting right on top of it, in a layer called the core-mantle-boundary or CMB.

The most pertinent way to model the CMB would be to track the fraction of silicates in every shell, since this would make the model more easily adjustable for modelling differentiation later on.

5.5 Silicate redistribution during dehydration

Since a model which contains both the rocky core and an icy mantle no longer benefits from preserving the mass of pure silicate in each shell, it is more pertinent to redefine the radii of the shells during each dehydrating time step. For this reason the mechanism for defining the boundaries of all the shells must be reconsidered during dehydration, since during this process the core itself contracts and the total radius may remain roughly the same or slightly contract as well, depending on the ice phase mantle model used.

The dehydration model described in section 1.5.2 gives the mass of hydrated silicates that gets dehydrated in a single time step by the latent heat of the process. This mass of hydrated silicate will be converted into dry silicate and water, of which the silicates are assumed to remain in the core and liquid is transported to the top of the core. Therefore the volume of the original dehydrating shell is then not completely full, but missing the volume of the liquid that is transported outwards. This deficit of volume is then filled by the silicates of the shell above, homogenising the density, heat capacity and conductivity. This refilling process is repeated for all shells from

the inside out until the entire new array of shells is filled. As discussed earlier, the total volume of the entire moon decreases, constituting a calculation of a new array of shells therefore volumes to fill up. So in addition to volumes of the post-dehydration moon needing to be refilled with the new phase in mind, the new volumes are also slightly smaller compared to the previous time step.

Since dehydration is in principle a phase change, the temperature in dehydrated shells remains at a constant 743K, keeping the temperatures of the resulting pure silicate and liquid the same. This requires setting the energies of the original dehydrating shells to a value that corresponds to the dehydrating temperature, to be redistributed and homogenised. However the silicate and liquid that is unaffected by dehydration would have its pre-dehydration energy gradient preserved, resulting in a temperature change only as a result of mixing with newly dehydrated materials, homogenising the properties in a single shell.

5.6 Differentiation

Using the process of tracking the fraction of silicates in the shell which contains the CMB, the mechanism could be expanded to model differentiation. Differentiation would be set up in the way of tracking the mass fraction of silicate in each shell and allowing for the materials to differentiate when melting is detected, similarly to the melting check described in section [3.5](#).

5.7 Initial conditions

A great way to develop the current work further would be to use the formation models of large icy moons to describe their internal properties for more accurate runs of the simulation code written in this work. Large icy moons are expected to be significantly hotter at the late formation stages, where this model becomes applicable, than the uniform value of 300 kelvins assumed in this work, making the final product of formation models the perfect initial conditions for running this code.

6 Conclusions

Large icy moons are a fascinating point of study due to their possible ability to heat up enough to melt some of the ice in their massive ice mantles and create oceans, which are considered to be the basis for life. Their most important method of heating is radiogenic heating, which is thoroughly modelled in this work. Incorporating the heating from several radioactive isotopes, this work assumes that Europa and Titan, the moons simulated here, are both differentiated into a rocky core and an ice mantle by the beginning of the simulation at 10 Myrs since the beginning of the solar system. Europa and Titan's cores are the main ones simulated since the other Galileian moons have cores that are similar in radius to Titan's, therefore do not constitute separate simulations.

The presence of water in the early stages of the moons' lifetime gives way to several processes also considered in this work, such as potassium leaching from the core into the ice mantle and hydration of the core. Potassium leaching is a very important effect in the large icy moons since the fraction of chondritic potassium remaining in the core greatly affects their temperature evolution since potassium-40 is the most important radiogenic element in heating the moon. However, since the remaining potassium fraction is still a subject of debate, several different possibilities were considered here, with the greatest remaining potassium fraction in Titan allowing the core to reach temperatures up to 3100 kelvins. Most simulations however were run with the often cited 30% of remaining potassium in any core, allowing Titan to reach a maximum temperature of 2100 kelvins over a time of 10 Gyrs.

Dehydration is also a very important chemical process considered in this work, since it is an endothermic reaction keeping the temperature at a constant 743 K for as long as it is ongoing, while also decreasing the total core radius due to the dehydrated liquid being transported to the ice mantle. If a core has a smaller amount of remaining potassium, like Titan and Europa are assumed to have, then dehydration takes a very long time, ending only a few hundred Myrs before present times for both. However, if Titan's core had retained all of its potassium, it would have dehydrated very early in its evolution in only about 200 Myrs.

It is important to note that the surface temperatures of all rocky cores simulated in this work were set to a constant value of 300 K, which defines the cooling of the cores' interiors. From a viewpoint of cooling over long time periods, moons that have a lower remaining potassium fraction begin cooling much later than those with more potassium. This is caused by the presence of radiogenic elements with longer lifetimes than the most important heat source of potassium-40, for example uranium (see the half-lives and heating rates of table [1](#)). When potassium leaching is substantial, then the initial heating, being still potassium-dominated, is later seamlessly succeeded by uranium, giving a combined effect of a more constant and long lived heating rate. With low amounts of potassium the overall temperatures reached are lower, as can be seen in figure [14](#) and since uranium is very long-lived it dominates the heating rate

of the silicate cores over long timescales.

The temperatures reached in the cores of Europa-like and larger moons are all very high, hence it is reasonable to say that all differentiate into a rocky core and ice mantle at some point in their lifetime. This is also possible, purely by radiogenic heating for Titan and Callisto as well, which have been postulated to not be fully differentiated at this point in time. Though it is important to keep in mind that if such large cores have a remaining potassium fraction even lower than 30% then it is possible for them to still be dehydrating, thus not using their heat to differentiate from the ice mantle.

One very interesting property of large icy moons is that even the cores with less potassium will at some point heat up enough to melt and begin convection in the core, thus allowing for full differentiation of metals from silicates, forming a metallic core. This is true even for moons with a smaller amount of potassium, though for those the metallic core would form in the future. This shows, however, that it is entirely possible for a metallic core to form, even for Europa, which has been debated to have one, and it is possible with only radiogenic heating as the heat source, excluding any possible tidal and gravitational heating.

In this thesis we have demonstrated the critical role of potassium leaching on the evolution of large icy moons. Over timescales up to present day in their evolution, the amount of potassium leached during the late formation stages largely defines the extent of dehydration and subsequent possible full differentiation in the cores of large icy moons. If there is less potassium remaining, the cores could still be undergoing dehydration and not heating the ice mantle from below, implying the lack of any liquid ocean, while a greater amount of potassium present in the core implies early and rapid dehydration with likely full differentiation into a metallic core occurring before present day. Several future space missions investigating the Galilean moons in depth, the JUICE mission and the Europa clipper are intended to give better constraints for the state of possible oceans in the large icy moons. Since these measurements will in part be done by changes in gravitational potential (Jara-Oru e and Vermeersen, 2016), these will give further insight into the state of differentiation in the Jovian moons. This would give a much clearer picture of the amount of potassium leaching present in the late formation stages, as the amount of leached potassium affects both the differentiation state of the core and the thickness of a liquid ocean.

References

- Barr, A. C. and Canup, R. M. (2008). Constraints on gas giant satellite formation from the interior states of partially differentiated satellites. *Icarus*, 198(1):163–177.
- Carlsaw, H. S. and Jaeger, J. C. (1959). *Conduction of heat in solids*. Clarendon Press.
- Castillo-Rogez, J. C. and Lunine, J. I. (2010). Evolution of Titan’s rocky core constrained by Cassini observations. *Geophys. Res. Lett.*, 37(20):L20205.
- Desch, S. J., Cook, J. C., Doggett, T. C., and Porter, S. B. (2009). Thermal evolution of Kuiper belt objects, with implications for cryovolcanism. *Icarus*, 202(2):694–714.
- Deschamps, F. and Sotin, C. (2001). Thermal convection in the outer shell of large icy satellites. *J. Geophys. Res.*, 106(E3):5107–5121.
- Elkins-Tanton, L. T., Weiss, B. P., and Zuber, M. T. (2011). Chondrites as samples of differentiated planetesimals. *Earth and Planetary Science Letters*, 305(1-2):1–10.
- Gao, P. and Stevenson, D. J. (2013). Nonhydrostatic effects and the determination of icy satellites’ moment of inertia. *Icarus*, 226(2):1185–1191.
- Grasset, O. and Sotin, C. (1996). The Cooling Rate of a Liquid Shell in Titan’s Interior. *Icarus*, 123(1):101–112.
- Hevey, P. J. and Sanders, I. S. (2006). A model for planetesimal meltdown by ^{26}Al and its implications for meteorite parent bodies. *Meteoritics and Planetary Science*, 41(1):95–106.
- Hobbs, P. (1974). *Ice Physics*. Clarendon Press.
- Hussmann, H., Sotin, C., and Lunine, J. I. (2015). *Interiors and Evolution of Icy Satellites*, volume 10, pages 605–635.
- Iess, L., Jacobson, R. A., Ducci, M., Stevenson, D. J., Lunine, J. I., Armstrong, J. W., Asmar, S. W., Racioppa, P., Rappaport, N. J., and Tortora, P. (2012). The Tides of Titan. *Science*, 337(6093):457.
- Jara-Oru e, H. and Vermeersen, B. (2016). Tides on jupiter’s moon ganymede and their relation to its internal structure. *Netherlands Journal of Geosciences - Geologie en Mijnbouw*, 95(2):191–201.
- Khurana, K. K., Kivelson, M. G., Stevenson, D. J., Schubert, G., Russell, C. T., Walker, R. J., and Polanskey, C. (1998). Induced magnetic fields as evidence for subsurface oceans in Europa and Callisto. *Nature*, 395(6704):777–780.
- Kirk, R. L. and Stevenson, D. J. (1987). Thermal evolution of a differentiated Ganymede and implications for surface features. *Icarus*, 69(1):91–134.

- Lodders, K. (2003). Solar System Abundances and Condensation Temperatures of the Elements. *ApJ*, 591(2):1220–1247.
- Néri, A., Guignard, J., Monnereau, M., Toplis, M. J., and Quitté, G. (2019). Metal segregation in planetesimals: Constraints from experimentally determined interfacial energies. *Earth and Planetary Science Letters*, 518:40–52.
- Neveu, M., Desch, S. J., and Castillo-Rogez, J. C. (2017). Aqueous geochemistry in icy world interiors: Equilibrium fluid, rock, and gas compositions, and fate of antifreezes and radionuclides. *Geochim. Cosmochim. Acta*, 212:324–371.
- Postberg, F., Schmidt, J., Hillier, J., Kempf, S., and Srama, R. (2011). A salt-water reservoir as the source of a compositionally stratified plume on Enceladus. *Nature*, 474(7353):620–622.
- Saur, J., Duling, S., Roth, L., Jia, X., Strobel, D. F., Feldman, P. D., Christensen, U. R., Retherford, K. D., McGrath, M. A., Musacchio, F., Wennmacher, A., Neubauer, F. M., Simon, S., and Hartkorn, O. (2015). The search for a subsurface ocean in Ganymede with Hubble Space Telescope observations of its auroral ovals. *Journal of Geophysical Research (Space Physics)*, 120(3):1715–1737.
- Schubert, G., Anderson, J. D., Spohn, T., and McKinnon, W. B. (2004). *Interior composition, structure and dynamics of the Galilean satellites*, volume 1, pages 281–306.
- Schubert, G., Anderson, J. D., Travis, B. J., and Palguta, J. (2007). Enceladus: Present internal structure and differentiation by early and long-term radiogenic heating. *Icarus*, 188(2):345 – 355.
- Solomatov, V. (2007). *Magma Oceans and Primordial Mantle Differentiation*, volume 9, pages 91–119.
- Spohn, T. and Schubert, G. (2003). Oceans in the icy Galilean satellites of Jupiter? *Icarus*, 161(2):456–467.
- Vilella, K., Limare, A., Jaupart, C., Farnetani, C. G., Fourel, L., and Kaminski, E. (2018). Fundamentals of laminar free convection in internally heated fluids at values of the Rayleigh-Roberts number up to 10^9 . *Journal of Fluid Mechanics*, 846:966–998.